DOI: 10.1002/chem.200902183

Photophysical Properties and OLED Applications of Phosphorescent Platinum(II) Schiff Base Complexes

Chi-Ming Che,*[a] Chi-Chung Kwok,[a] Siu-Wai Lai,[a] Andreas F. Rausch,[b] Walter J. Finkenzeller,[b] Nianyong Zhu,[a] and Hartmut Yersin*[b]

Abstract: The syntheses, crystal structures, and detailed investigations of the photophysical properties of phosphorescent platinum(II) Schiff base complexes are presented. All of these complexes exhibit intense absorption bands with λ_{max} in the range 417–546 nm, which are assigned to states of metal-to-ligand charge-transfer (^{1}MLCT) ^{1}[Pt(5d)→π*(Schiff base)] character mixed with ^{1}[lone pair(phenoxide)→π*(imine)] charge-transfer character. The platinum(II) Schiff base complexes are thermally stable, with decomposition temperatures up to 495 °C, and show emission λ_{max} at 541–649 nm in acetonitrile, with emission quantum yields up to 0.27. Measurements of the emission decay times in the temperature range from 130 to 1.5 K give total zero-field splitting parameters of the emitting triplet state of 14–28 cm^{-1}. High-performance yellow to red organic light-emitting devices (OLEDs) using these platinum(II) Schiff base complexes have been fabricated with the best efficiency up to 31 $cd\,A^{-1}$ and a device lifetime up to 77000 h at 500 $cd\,m^{-2}$.

Keywords: organic light-emitting diodes · phosphorescence · platinum · Schiff bases · triplet state

Introduction

Transition-metal complexes with long-lived and emissive excited states are increasingly used in the design of functional molecular materials. In this regard, phosphorescent d^6 and d^8 metal complexes containing π-conjugated ligands with N and/or C donor atoms have been extensively studied and used in the development of high-performance organic light-emitting diodes (OLEDs).[1] In contrast, the materials applications of transition-metal Schiff base complexes are less developed, even though Schiff base ligands are easily prepared and structurally modified, and have been demonstrated to have immense practical applications, such as in the development of metal catalysts for highly enantioselective organic transformation reactions.[2] The electroluminescent properties of zinc(II) complexes bearing bidentate azomethine and tetradentate Schiff base ligands had been reported by Sano and Liu,[3] and were used in the fabrication of blue and green OLEDs. Recently, conjugated polymers containing zinc(II) and nickel(II) Schiff base complexes have been reported to have OLED applications.[4] As the synthetic chemistry of Schiff base metal complexes is prevalent, the exploration of their photophysical and photochemical properties, and materials applications, could provide access to new classes of functional molecular materials of practical interest.

In the past several years, we and others have reported the applications of thermally stable, phosphorescent platinum(II) emitters as electrophosphorescent dopant materials,[1b,5] and we communicated that platinum(II) Schiff base complexes could be used for high-performance OLEDs.[6] In this study, we present a detailed account of the photophysical and electroluminescent properties of platinum(II) Schiff base complexes, revealing that these complexes are attractive candidates for electrophosphorescent applications.

[a] Prof. Dr. C.-M. Che, Dr. C.-C. Kwok, Dr. S.-W. Lai, Dr. N. Zhu
Department of Chemistry and
HKU-CAS Joint Laboratory on New Materials
The University of Hong Kong
Pokfulam Road, Hong Kong SAR (China)
Fax: (+852) 2857-1586
E-mail: cmche@hku.hk

[b] Dipl.-Chem. A. F. Rausch, Dr. W. J. Finkenzeller, Prof. Dr. H. Yersin
Institut für Physikalische und Theoretische Chemie
Universität Regensburg, 93040 Regensburg (Germany)
Fax: (+49) 941-943-4488
E-mail: hartmut.yersin@chemie.uni-regensburg.de

Results

Synthesis and characterization: The preparation of platinum(II) Schiff base complexes has been reported previously.[7,8] In this work, we have modified the synthetic procedures developed by Shagisultanova and co-workers for the preparation of complexes **1a**–**8b** (Scheme 1). Treatment of

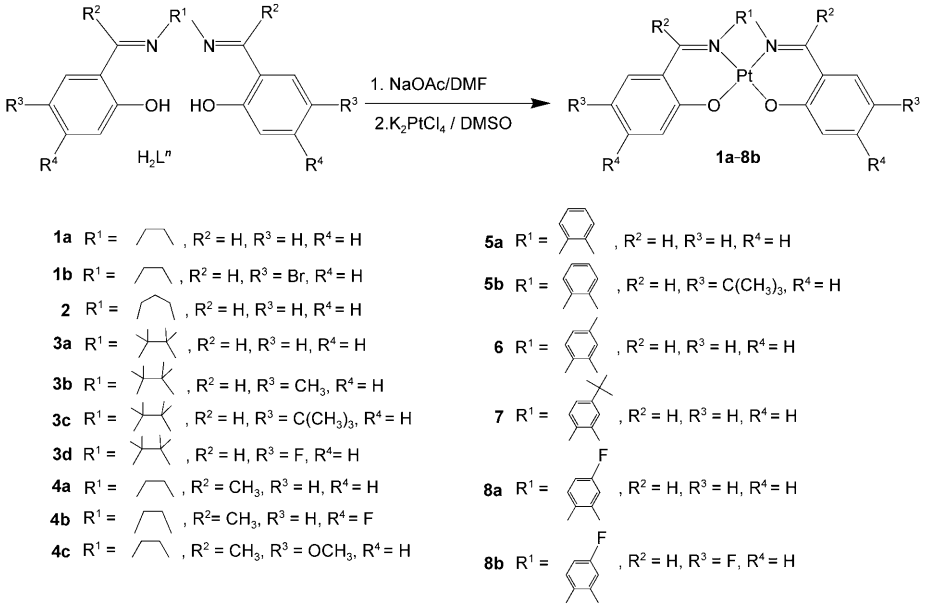

Scheme 1. Synthetic scheme for Pt^{II} Schiff base complexes from ligands H_2L^n ($n=1$ a–8b).

K_2PtCl_4 with Schiff base ligands (H_2L^{1a}–H_2L^{3a}) in aqueous KOH solution (1 M) under argon atmosphere was followed by purification, which afforded **1a**–**3a** as orange crystalline solids. Attempts to use the bulky Schiff base ligand (*R*,*R*)-(−)-*N*,*N*′-bis(3,5-di-*tert*-butylsalicylidene)-1,2-cyclohexanediamine in the synthesis were not successful; presumably the insolubility of this Schiff base ligand in aqueous KOH solution could present a problem. We further modified the method by using a basic medium: a solution of K_2PtCl_4 in DMSO was added to a solution of Schiff base in DMF containing sodium acetate. The procedures were subsequently followed for synthesizing the platinum(II) Schiff base complexes in this work; and can be used for gram-scale synthesis. As an example, 10 g of complex **5a** was prepared by this method in a one-pot reaction. Complexes **1a**–**8b** are stable in the solid state, and no decomposition or ligand dissociation was observed in EtOH, 2-propanol, DMSO, or CH_3CN under ambient conditions for one month.

X-ray crystal structures: The crystal structures of **3d**, **5a**·DMF, and **7**·CH_2Cl_2 have been determined (Figures 1–3 and Table 1); the X-ray crystal structure of **1a** was reported previously[9] and that of **3a** was communicated by us earlier.[6] The platinum atom resides in a square-planar geometry. The average Pt–N distances of 1.946, 1.970, and 1.955 Å for **3d**, **5a**, and **7**, respectively, resemble those in **1a** (1.944 Å)[9] and **3a** (1.941 Å).[6] The mean Pt–O distances of **3d**, **5a**, and **7** are 1.990, 1.994, and 2.000 Å respectively, which are also comparable to those reported for **1a** (2.004 Å),[9] **3a** (1.989 Å),[6] and those platinum(II) complexes bearing tetradentate bis(phenoxy)diimine ligands, [Pt(*t*$Bu_2N_2O_2$)] (1.975 Å) and [Pt($Ph_2N_2O_2$)] (1.978 Å) (*t*$Bu_2N_2O_2H_2$ = 6,6′-bis(2″-hydroxyphenyl)-4,4′-bis-(*tert*-butyl)-2,2′-bipyridine and $Ph_2N_2O_2H_2$ = 2,9-bis(2′-hydroxyphenyl)-4,7-diphenyl-1,10-phenanthroline).

In the reported crystal structure of **1a**, the molecules are arranged in pairs in a head-to-tail fashion with Pt···Pt distances of 3.277(1) Å,[9] which are in the range of 2.7–3.5 Å. Thus, weak Pt^{II}···Pt^{II} interactions might be possible.[5i,10,11] In contrast, the shortest Pt···Pt distances are 5.922 and 6.806 Å in the crystal structures of **3a** and **3d**, respectively. These are attributed to the bulky tetramethylethylene moiety, which disfavors close intermolecular interactions. There are short intermolecular contacts between *tert*-butyl groups and phenoxide moieties

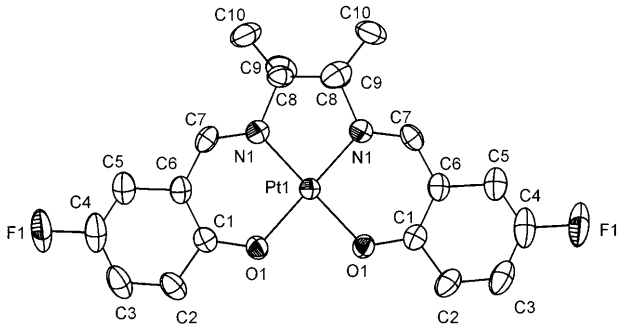

Figure 1. Perspective view of **3d** (30% probability ellipsoids, hydrogen atom labels omitted for clarity). Selected bond lengths (Å): Pt1–N1 1.946(4), Pt1–O1 1.990(3). Selected bond angles (°): N1-Pt1-O1 95.3(2), N1-Pt1-$N1^i$ 84.4(3), N1-Pt1-$O1^i$ 177.4(1).

(C–H···O 2.392 Å; C–H···C(aryl) 2.880 Å) in the crystal structure of **3d**, whereas the closest intermolecular aryl π–π separation is 3.307 Å.

Figure 2 (top) shows that **5a** has a planar geometry with negligible distortion of aryl rings from the PtN_2O_2 plane. Bond lengths and angles are consistent with those reported for typical platinum(II) Schiff base complexes,[6,9] and the bond angles at the platinum atom (N1-Pt1-N2, N1-Pt1-O1,

Table 1. Crystal data and structure refinement for **3d**, **5a**·DMF, and **7**·CH_2Cl_2.

	3d	**5a**·DMF	**7**·CH_2Cl_2
formula	$C_{20}H_{20}F_2N_2O_2Pt$	$C_{23}H_{21}N_3O_3Pt$	$C_{25}H_{24}Cl_2N_2O_2Pt$
M_r	553.47	582.52	650.45
crystal system	tetragonal	monoclinic	monoclinic
space group	P 4_3 2_1 2	P 2_1/c	P 2_1/c
a [Å]	11.342(2)	11.900(2)	14.946(3)
b [Å]	11.342(2)	14.180(3)	14.046(3)
c [Å]	15.047(3)	12.078(2)	12.410(3)
α [°]	90	90	90
β [°]	90	95.41(3)	106.71(3)
γ [°]	90	90	90
V [Å^3]	1935.7(5)	2029.0(7)	2495.2(9)
Z	4	4	4
ρ_{calcd} [g cm^{-3}]	1.899	1.907	1.731
μ ($Mo_{K\alpha}$) [mm^{-1}]	7.284	6.946	5.861
crystal size [mm^3]	0.50×0.35×0.20	0.30×0.20×0.10	0.50×0.30×0.20
$2\theta_{max}$ [°]	50.78	51.82	50.92
unique reflns	1789	3728	4411
obsvd data [$I>2\sigma(I)$]	1455	2888	2767
$R^{[a]}$, $R_w^{[b]}$	0.024, 0.058	0.034, 0.078	0.040, 0.098
residual ρ [e Å^{-3}]	+0.94, −0.28	+1.89, −1.65	+0.97, −0.94

[a] $R=\Sigma||F_o|-|F_c||/\Sigma|F_o|$. [b] $R_w=[\Sigma w(|F_o|-|F_c|)^2/\Sigma w|F_o|^2]^{1/2}$.

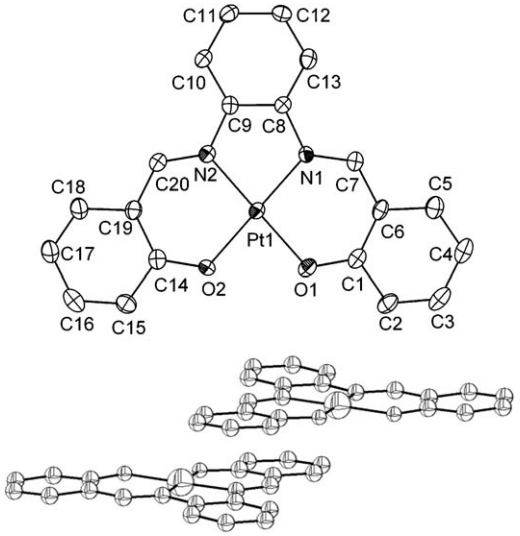

Figure 2. Top: Perspective view of **5a** (30% probability ellipsoids, hydrogen atom labels omitted for clarity). Selected bond lengths (Å): Pt1−N1 1.965(4), Pt1−N2 1.976(4), Pt1−O1 1.992(4), Pt1−O2 1.996(4). Selected bond angles (°): N1-Pt1-N2 83.5(2), N1-Pt1-O1 96.1(2), N2-Pt1-O2 96.1(2), O1-Pt1-O2 84.3(2), N2-Pt1-O1 178.9(2), N1-Pt1-O2 179.2(2); Bottom: Crystal packing diagram showing π–π interactions.

N2-Pt1-O2, and O1-Pt1-O2) lie in the range of 83.5–96.1°. In the crystal structure of **5a** (Figure 2, bottom), the molecules are in pairs in a head-to-tail fashion. There are π–π interactions between phenylene (R^1) and phenoxide groups. The intermolecular (imine)N=C···C(phenylene) and π–π (phenylene–phenoxide) distances are 3.339 and 3.348 Å, respectively, whereas the intermolecular Pt···Pt separation is 6.368 Å. The DMF molecules have H_2C−H···O(phenoxide) (2.658 Å), H_2C−H···C(phenoxide) (2.839 Å), C=O···H−C(phenylene) (2.639 Å), C=O···H−C=N(imine) (2.282 Å), C=O···CH=N(imine) (3.161 Å), and C=O···H−C(phenoxide) (2.574 Å) contacts.

The structure of **7** (Figure 3, top) is similar to **5a** except for the *tert*-butyl group in the phenylene moiety. The molecules are arranged in a head-to-tail fashion as similarly observed for **5a** (Figure 3, bottom), regardless of the bulky *tert*-butyl substituent. The intermolecular (imine)N=C···C(phenoxide) and π–π (phenylene–phenoxide) distances are 3.398 and 3.387 Å, respectively, and the intermolecular Pt···Pt separation is 4.901 Å. For **5a** and **7**, the interplanar separations are 3.339–3.398 Å, which are close enough for allowing phenylene (R^1) and phenoxide groups to have intermolecular π–π stacking interactions.[5i,9–11]

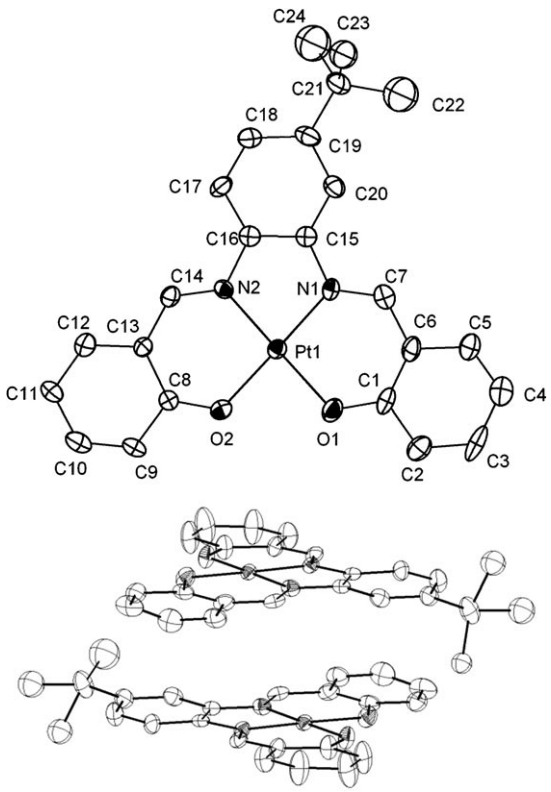

Figure 3. Top: Perspective view of **7** (30% probability ellipsoids, hydrogen atom labels omitted for clarity). Selected bond lengths (Å): Pt1−N1 1.957(6), Pt1−N2 1.953(6), Pt1−O1 2.002(5), Pt1−O2 1.997(5). Selected bond angles (°): N1-Pt1-N2 83.4(3), N1-Pt1-O1 95.9(3), N2-Pt1-O2 95.7(2), O1-Pt1-O2 85.1(2), N1-Pt1-O2 178.6(2), N2-Pt1-O1 178.4(2); Bottom: Crystal packing diagram indicating π–π interactions.

Thermal stability: The thermal stabilities of **1a–8b** were examined by thermogravimetric analysis (TGA) under nitrogen atmosphere (Table 2). All complexes have high thermal stability; the decomposition temperature ranges from 315°C (**1b**) to 495°C (**3c**). For **3a–3d** bearing the tetramethylethylene (R^1) motif, replacing the R^3 substituent in the two phenoxide moieties from H to CH_3, *t*Bu, or F leads to a significant increase in the decomposition temperature (T_d) from 382 to 474–495°C. Similarly, changing R^3 from H in **4a**

Table 2. Physical properties for complexes **1a**–**8b**.

	E_{pa} [V][a]	E_{pc} [V][a]	HOMO [eV][b]	LUMO [eV][c]	T_d [°C][d]
1a	0.52	−2.46	−5.32	−2.34	406
1b	0.54	−2.32	−5.34	−2.48	315
2	0.52	−2.48	−5.32	−2.32	369
3a	0.86	−2.74	−5.66	−2.06	382
3b	0.65	−2.57	−5.45	−2.24	474
3c	0.67	−2.55	−5.47	−2.25	495
3d	0.78	−2.46	−5.58	−2.34	484
4a	0.47	−2.72	−5.27	−2.08	345
4b	0.46	−2.59	−5.26	−2.21	379
4c	0.43	–	−5.23	–	455
5a	0.57	−1.82	−5.37	−2.89	415
5b	0.60	−1.92	−5.40	−2.88	339
6	0.54	−1.84	−5.34	−2.96	411
7	0.55	−1.87	−5.35	−2.93	396
8a	0.59	−1.80	−5.39	−3.00	414
8b	0.35	−1.79	−5.15	−3.01	408

[a] Versus ferrocene/ferrocenium couples. [b] Estimated from the oxidation potentials. [c] Estimated from the reduction potentials. [d] Determined by TGA.

to OCH_3 in **4c** leads to an increase in T_d from 345 to 455 °C. However, when the R^4 substituents in the phenoxide groups change from H (**4a**) to F (**4b**), there is no significant effect on the T_d values.

No glass transition was observed in differential scanning calorimetric experiments (DSC) for **1a**–**8b** up to 300 °C, revealing that the glass-transition temperatures (T_g) of these platinum(II) complexes are above 300 °C.

Electrochemistry: Cyclic voltammograms of **1a**–**8b** were recorded in degassed DMF with 0.1 M tetrabutylammonium hexafluorophosphate (TBAP) as supporting electrolyte. All potentials are referenced to the ferrocenium–ferrocene [$E°(FeCp_2^{+/0})$] couple. In each case (except **4c**), there is one irreversible anodic wave with E_{pa} at 0.35–0.86 V and one irreversible cathodic wave with E_{pc} at −1.79 to −2.74 V. Both the anodic and cathodic waves are attributed to the oxidation and reduction, respectively, of Schiff base ligands. The HOMO and LUMO levels of these complexes were estimated from the oxidation and reduction potentials to be −5.15 to −5.66 eV and −2.06 to −3.01 eV, respectively.

Electronic absorption spectroscopy: The UV/Vis absorption spectral data of **1a**–**8b** are listed in Table 3. As examples, the absorption spectra of **1a**, **3a,** and **5** in acetonitrile and the absorption spectrum of **1b** in DMF are given in Figure 4. In acetonitrile, the absorption spectra of **1b**, and **3a**–**4c**, having the aliphatic R^1 motif, are similar to that of **1a**, each comprising intense high-energy absorption bands at λ_{max} = 306–352 nm ($\varepsilon \approx (1.09–1.59)\times10^4$ dm^3 mol^{-1} cm^{-1}), moderately intense absorption bands at λ_{max} = 394–439 nm ($\varepsilon \approx (0.47–0.66)\times10^4$ dm^3 mol^{-1} cm^{-1}) and weak absorption shoulders at λ_{max} = 465–535 nm ($\varepsilon \approx$ 60–80 dm^3 mol^{-1} cm^{-1}). Complexes with the phenylene R^1 motif (**5**–**8b**) show two high-energy absorptions with peak maxima at λ_{max} = 311–316 nm ($\varepsilon \approx (1.43–2.16)\times10^4$ dm^3 mol^{-1} cm^{-1}) and λ_{max} = 357–379 nm ($\varepsilon \approx (2.45–3.57)\times10^4$ dm^3 mol^{-1} cm^{-1}), plus two moderately intense absorption bands at λ_{max} = 451–467 nm ($\varepsilon \approx (0.58–0.76)\times10^4$ dm^3 mol^{-1} cm^{-1}) and λ_{max} = 520–546 nm ($\varepsilon \approx (0.60–0.80)\times10^4$ dm^3 mol^{-1} cm^{-1}). The absorbance of **3a** at λ_{max} = 413 nm obeys Beer's law with the complex concentration in the range of 1×10^{-5} to 2×10^{-4} mol dm^{-3}, revealing no oligomerization under this condition. As depicted in Figure 5 (top), the absorption band of **3a** at λ_{max} = 413 nm in MeOH is red-shifted to longer wavelength, and is resolved

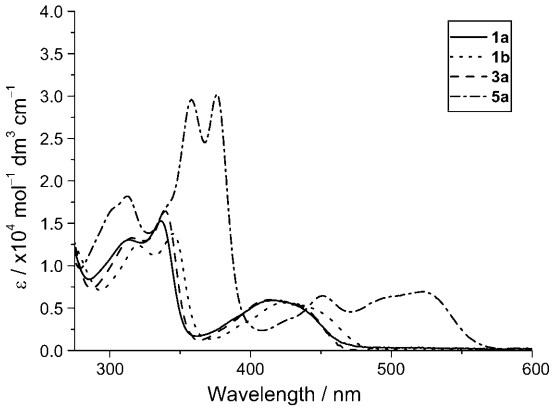

Figure 4. Absorption spectra of **1a**, **3a**, and **5a** in CH_3CN and **1b** in DMF.

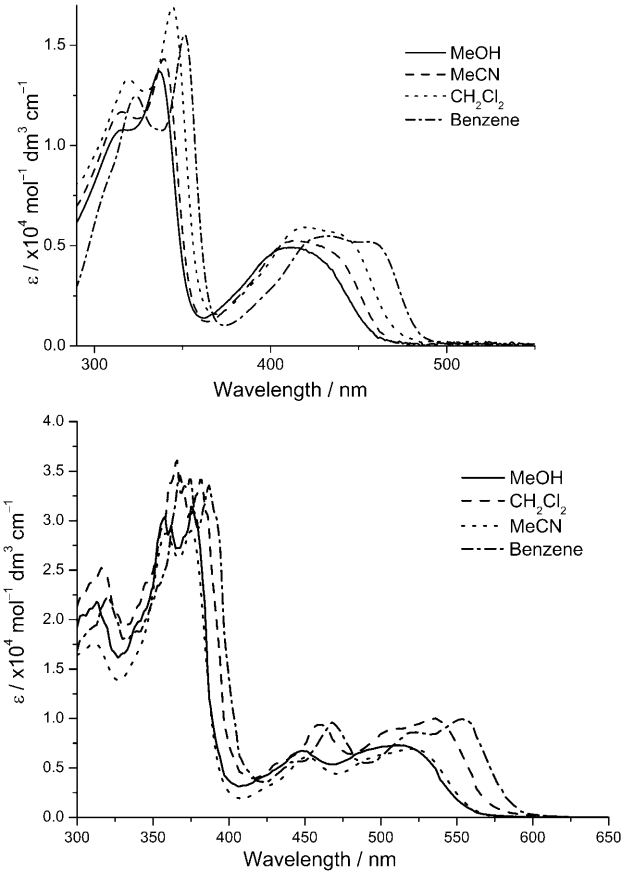

Figure 5. Absorption spectra of **3a** (top) and **5a** (bottom) in various solvents.

Table 3. Photophysical data of complexes **1a**–**8b**.

	Medium (T [K])	λ_{abs} [nm] (ε [$mol^{-1}dm^3cm^{-1}$])	λ_{em}[a] [nm]	τ [μs]	k_q [10^8 $mol^{-1}dm^3s^{-1}$]	Φ_{em}
1a	CH_3CN (298)	250 (46200), 314 (13000), 336 (15300), 417 (5900), 503 (sh, 80)	550, 580 (sh)	3.5	4.7	0.19
	solid (298)		548 (max), 594, 648 (sh)	0.2		
	solid (77)		564 (max), 619	3.0		
	glass (77)[b]		521 (max), 565, 615 (sh)	10.7		
1b	DMF (298)	319 (12400), 345 (13500), 424 (5600)	560	2.4	4.4	0.14
	solid (298)		564 (max), 603	0.2		
	solid (77)		564 (max), 612	2.4		
	glass (77)[b]		534 (max), 580, 632 (sh)	8.3		
2	CH_3CN (298)	250 (40800), 320 (sh, 9600), 340 (11200), 420 (5100), 500 (sh, 60)	592	0.46	1.7	0.087
	solid (298)		598	–[c]		
	solid (77)		612	0.74		
	glass (77)[b]		521 (max), 560	6.5		
3a	CH_3CN (298)	246 (46000), 316 (11600), 339 (14200), 413 (5300), 432 (sh, 4800), 501 (sh, 60)	541, 580 (sh)	3.4	4.3	0.18
	MeOH (298)	245 (42800), 317 (10800), 337 (13800), 411 (5000), 430 (sh, 4300), 492 (80)	537	3.4		0.17
	CH_2Cl_2 (298)	319 (13100), 344 (16700), 420 (5800), 440 (5400)	542	3.7		0.27
	benzene (298)	323 (12600), 351 (15300), 433 (5500), 455 (5200)	546	3.9		0.27
	solid (298)		551 (max), 585	1.49		
	solid (77)		544 (max), 589	6.4		
	glass (77)[b]		514 (max), 555, 595 (sh)	10.3		
3b	CH_3CN (298)	252 (50100), 317 (13700), 346 (15700), 427 (6000), 446 (sh, 5600), 520 (70)	556	2.88	1.3	0.23
	solid (298)		552 (max), 589, 644 (sh)	0.15		
	solid (77)		560 (max), 610, 669 (sh)	5.02		
	glass (77)[b]		520 (max), 564, 617 (sh)	10.2		
3c	CH_3CN (298)	251 (50900), 316 (13500), 345 (15900), 423 (5700), 440 (sh, 5300), 514 (70)	551	3.81	1.1	0.26
	solid (298)		564 (max), 601, 660 (sh)	2.08		
	solid (77)		553 (max), 603, 665	5.5		
	glass (77)[b]		516 (max), 558, 610	11.8		
3d	CH_3CN (298)	245 (37800), 320 (11600), 346 (12100), 429 (5200), 448 (sh, 5000), 529 (70)	568	2.32	0.89	0.13
	solid (298)		564 (max), 599	0.43		
	solid (77)		548 (max), 596, 651 (sh)	1.38		
	glass (77)[b]		538 (max), 587, 647 (sh)	8.41		
4a	CH_3CN (298)	252 (32300), 319 (sh, 10500), 337 (12400), 409 (4700), 426 (sh, 1400), 493 (60)	548	1.68	8.6	0.08
	solid (298)		542, 579 (max), 622 (sh)	–[c]		
	solid (77)		543 (max), 583, 622 (sh)	1.72		
	glass (77)[b]		518 (max), 558, 600 (sh)	11.8		
4b	CH_3CN (298)	249 (40000), 306 (14000), 324 (14000), 394 (6600), 465 (80)	552	1.57	3.1	0.07
	solid (298)		514, 549 (max), 592, 640 (sh)	0.73		
	solid (77)		512, 556 (max), 591, 636 (sh)	2.11		
	glass (77)[b]		510 (max), 551, 598 (sh)	16.0		
4c	CH_3CN (298)	242 (37700), 316 (10900), 352 (11100), 439 (5500), 458 (sh, 4900), 535 (50)	588	2.31	2.3	0.08
	solid (298)		587 (max), 626	–[c]		
	solid (77)		599 (max), 616, 647, 660	4.9		
	glass (77)[b]		542 (max), 569, 586, 615 (sh)	12.0		

Table 3. (Continued)

	Medium (T [K])	λ_{abs} [nm] (ε [$mol^{-1}dm^3cm^{-1}$])	λ_{em}[a] [nm]	τ [μs]	k_q [10^8 $mol^{-1}dm^3s^{-1}$]	Φ_{em}
5a	CH_3CN (298)	250 (34900), 312 (18200), 358 (29900), 376 (30700), 451 (6500), 504 (sh, 6500), 523 (7100)	611	3.43	6.9	0.23
	MeOH	245 (37300), 314 (21600), 358 (30400), 377 (31100), 448 (7060), 515 (6800)	608	1.4		0.10
	CH_2Cl_2	253 (41600), 318 (24900), 366 (36100), 382 (34100), 462 (9300), 503 (sh, 8600), 535 (9900)	618	3.6		0.20
	benzene	243 (50600), 321 (22200), 367 (34600), 387 (33600), 468 (9600), 519 (8600), 554 (9900)	628	3.1		0.26
	solid (298)		626, 672 (sh)	0.42		
	solid (77)		623, 644 (max), 666	3.09		
	glass (77)[b]		590 (max), 645, 714 (sh)	11.0		
5b	CH_3CN (298)	255 (41700), 316 (18800), 361 (33100), 379 (35700), 460 (7100), 532 (7200)	625	4.62	5.9	0.27
	solid (298)		668	–[c]		
	solid (77)		670	2.62		
	glass (77)[b]		601 (max), 661, 730 (sh)	10.6		
6	CH_3CN (298)	250 (37200), 315 (19400), 357 (30900), 375 (32200), 453 (7300), 521 (7300)	611	3.2	5.4	0.18
	solid (298)		630, 694 (sh)	0.39		
	solid (77)		638, 694 (sh)	1.58		
	glassy (77)[b]		590 (max), 649, 718 (sh)	10.1		
7	CH_3CN (298)	250 (40500), 315 (21600), 357 (32900), 375 (34300), 453 (7600), 520 (8000)	610	4.54	7.8	0.23
	solid (298)		630, 691 (sh)	–[c]		
	solid (77)		651, 715 (sh)	2.86		
	glass (77)[b]		590 (max), 648	10.5		
8a	CH_3CN (298)	248 (32500), 311 (15100), 360 (27100), 378 (27300), 455 (5800), 523 (6000)	615	4.43	18	0.21
	solid (298)		647	0.45		
	solid (77)		674	3.78		
	glass (77)[b]		600, 654 (sh)	13.5		
8b	CH_3CN (298)	244 (27700), 314 (14300), 361 (24500), 377 (26400), 467 (5800), 516 (sh, 5900), 546 (6500)	649	2.87	25	0.07
	solid (298)		681	–[c]		
	solid (77)		706	0.52		
	glass (77)[b]		624, 692 (sh)	10.2		

[a] Excitation wavelength at $\lambda_{max} > 390$ nm. [b] Measured in MeOH/EtOH = 1:4. [c] Lifetime cannot be detected due to weak emission.

into two broad absorption peak maxima at 433 and 455 nm in benzene. A similar solvent effect on the absorption spectrum of **5a** was found. As depicted in Figure 5 (bottom), its low-energy absorption band at $\lambda_{max} = 512$ nm in MeOH is red-shifted, and resolved to peak maxima with $\lambda_{max} = 519$ and 554 nm in the less polar solvent, benzene.

Emission spectroscopy: The emission spectra of **1a–8b** with complex concentrations of 10^{-5} M in solution are depicted in Figure 6. Intense emission bands with λ_{max} at 541–592 nm ($\Phi = 0.07$–0.26; $\tau = 0.46$–3.5 μs) are observed upon excitation of the platinum(II) complexes having an aliphatic R^1 motif (**1a**, **1b**, **3a–4c**) at ≈400 nm in CH_3CN at 298 K. The time-resolved absorption spectrum of the emissive triplet excited state of **3a** in degassed CH_3CN was recorded (Figure 7). The spectrum features an absorption band at ≈480 nm, and the measured decay lifetime of 3.6 μs closely matches the emission lifetime in CH_3CN, revealing that the emission band originates from the triplet emissive excited state.

In the solid state, the emission bands of **1a**, **1b**, **2**, and **3a–4c** show λ_{max} at 548–598 nm ($\tau \leq 2.08$ μs) at 298 K and at 543–612 nm ($\tau = 1.38$–6.4 μs) at 77 K. At 77 K in glassy MeOH/EtOH (1:4) solutions, their emission maxima blue-shift to 510–542 nm from the respective solid-state emission maxima at 543–612 nm, and the emission lifetimes are 6.5–16 μs. In CH_3CN at 298 K, complexes **5a–8b** with phenylene

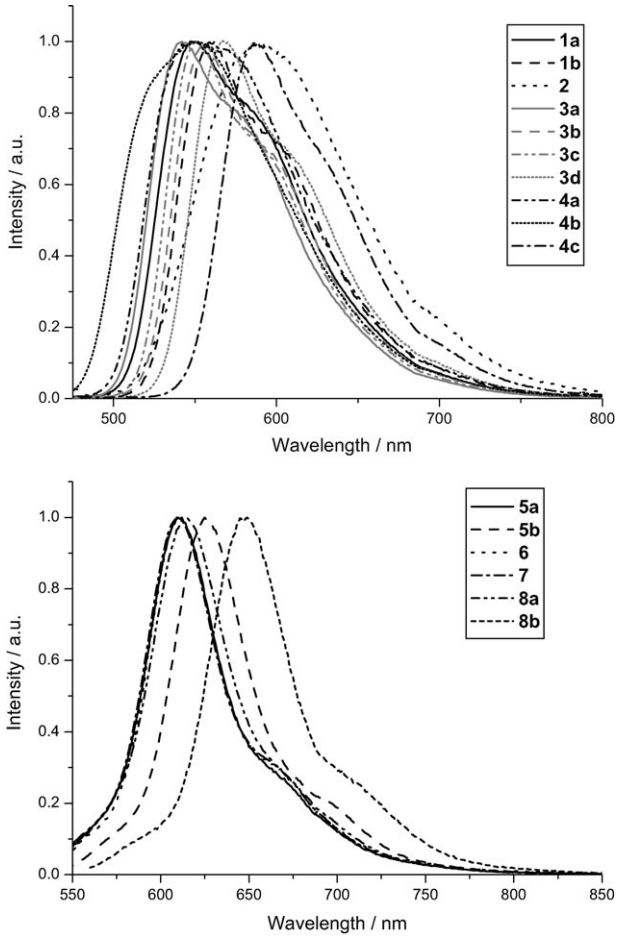

Figure 6. Solution emission spectra for **1a**–**8b** in CH_3CN (except **2** in DMF).

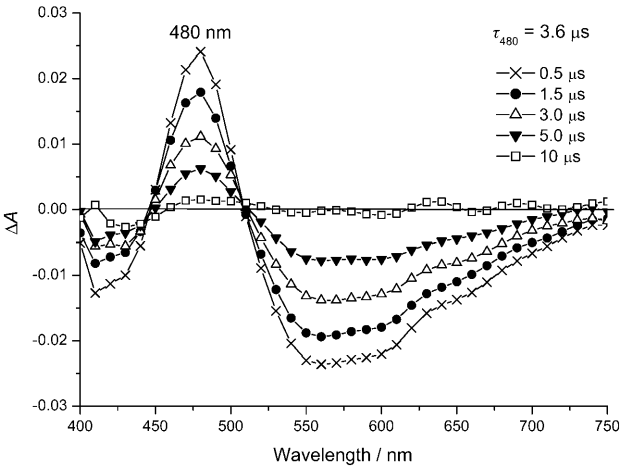

Figure 7. Time-resolved difference absorption spectra of **3a** in CH_3CN.

R^1 motif show a red emission with λ_{max} at 610–649 nm and with emission quantum yields and lifetimes being Φ_{em} = 0.07–0.27 and τ = 2.87–4.62 μs, respectively. The solid-state emission λ_{max} of **5a**–**8b** are at 626–681 nm at 298 K and 638–706 nm at 77 K; all of these emissions decay with $\tau \leq 3.8$ μs. At 77 K in glassy MeOH/EtOH (1:4), the emission λ_{max} are at 590–624 nm (τ = 10.1–13.5 μs). Self-quenching of the emissions of **1a**–**8b** with concentrations of the metal complexes of 1×10^{-5} to 5×10^{-3} mol dm^{-3} is evident in CH_3CN (except **1b** in DMF). At 298 K, linear plots of $1/\tau$ versus complex concentration were obtained and the k_q values were determined to be 8.9×10^7 (**3d**)–2.5×10^9 mol^{-1} dm^3 s^{-1} (**8b**); the results are depicted in Table 3. The emission of **3a** shows smaller solvatochromatic effects than observed for the absorption. Its emission maximum in MeOH is at 537 nm (18620 cm^{-1}), which is red-shifted to 546 nm by only 310 cm^{-1} in benzene (18310 cm^{-1}). A similar solvatochromatic effect is observed for **5a**: its emission maximum is red-shifted by only 520 cm^{-1} when the solvent changes from MeOH to benzene.

Temperature-dependent emission lifetimes and zero-field splitting (ZFS) parameters: Significant splitting of a triplet state of an organo-transition-metal compound is only present if effective spin-orbit coupling (SOC) provides mixing of the T_1 substates with higher-lying singlets and triplets of MLCT character.[12–14] This mixing is responsible not only for the amount of ZFS, but also for the variation of many other photophysical properties.[15,16] In particular, SOC provides a softening of the spin-forbiddenness of the transitions between the T_1 substates and the singlet ground state S_0. Thus, a desired reduction of the radiative emission decay time is induced. The amount of ZFS can be utilized to classify the degree of MLCT perturbation and SOC efficiency in the emitting triplet state. An empirical ordering scheme developed by Yersin et al.[15–18] for organo–transition-metal triplet emitters provides a useful scale for an assessment of the MLCT perturbation in the T_1 state. Furthermore, the ZFS parameters also give an indication concerning the suitability of a compound for application as an emitter in OLEDs, since all efficient triplet emitters hitherto studied exhibit ΔE(ZFS) values of theT_1 state larger than about 10 cm^{-1}.[12] Therefore, it is of great interest to determine this important parameter for the complexes described in this work. Besides the direct determination of the ZFS parameters from highly resolved emission and excitation spectra,[12,16,17] it is possible to obtain these values from the temperature dependence of the emission decay time. Under the assumption of fast thermalization, the occupation dynamics of the excited states (triplet substates) involved in the emission process are governed by Equation (1),[12,19–21] in which n_i denotes the Boltzmann occupation number of state i, k_i is the total rate constant for depopulation of state i. N is the total number of occupied excited states and $k_{therm} = 1/\tau_{therm}$ is the rate constant for depopulation of the equilibrated system of excited states, that is, the inverse of the measured decay time.

$$\frac{dN}{dt} = -k_{therm}N = -\sum_i k_i n_i \qquad (1)$$

Considering emission from the lowest triplet state T_1, i can be one of the triplet substates I, II, or III. Introduction

of Boltzmann factors to Equation (1) results in an expression that describes the temperature dependence of the measured decay time in a model of three excited states, given in Equation (2).[12,19–21]

$$k_{\mathrm{therm}} = \frac{k_{\mathrm{I}} + k_{\mathrm{II}} e^{-\Delta E_{\mathrm{II,I}}/k_{\mathrm{B}}T} + k_{\mathrm{III}} e^{-\Delta E_{\mathrm{III,I}}/k_{\mathrm{B}}T}}{1 + e^{-\Delta E_{\mathrm{II,I}}/k_{\mathrm{B}}T} + e^{-\Delta E_{\mathrm{III,I}}/k_{\mathrm{B}}T}} \qquad (2)$$

$\Delta E_{\mathrm{II,I}}$ and $\Delta E_{\mathrm{III,I}}$ are the energy differences between the triplet substates II and I, and III and I, respectively; k_B is the Boltzmann constant. By fitting Equation (2) to the measured decay times, one can obtain the ΔE(ZFS) values and the individual decay times of the triplet sublevels τ_{I}, τ_{II}, and τ_{III}. These parameters are visualized in the energy level diagram depicted in Figure 8.

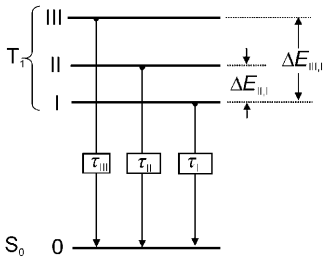

Figure 8. Schematic energy-state diagram for the substates of the emitting T_1 state of organo–transition-metal compounds. τ_{I}, τ_{II}, τ_{III} represent the individual (radiative and non-radiative) decay times from the substates. $\Delta E_{\mathrm{II,I}}$ and $\Delta E_{\mathrm{III,I}}$ are the zero-field splitting parameters between the substates.

Complexes **3a**, **3c**, **3d**, **4b**, and **5a** were chosen for an assessment of the individual properties of the triplet substates. The emission decay of all these five platinum(II) Schiff base complexes in polycrystalline tetrahydrofuran (THF) was monoexponential in the temperature range of $1.5 \leq T \leq 130$ K. At higher temperatures, additional non-radiative processes became effective as the melting point of the solvent was reached. The complexes **3a** and **5a** were additionally investigated in glassy EtOH.

The measured decay data for **3a** in THF, along with a fit of Equation (2) to the experimental data, are shown in Figure 9. At $T \leq 1.5$ K, the plot of decay time versus temperature maintains a plateau with a decay time of $\tau_{\mathrm{I}} = 83$ μs. In this range, the emission stems from the lowest triplet substate I. According to the relatively long decay time, it can be concluded that the transition I→0 is strongly forbidden. As the temperature is increased, the measured emission lifetime is drastically reduced. This behaviour shows that higher lying triplet substates with higher decay rates are thermally populated. The decay time at temperatures $T > 100$ K is (due to its short decay time) mainly governed by the emission of substate III. Based on data fitting of the measured emission decay times, the individual triplet sublevel decay times τ_{I}, τ_{II}, and τ_{III} and the zero-field splitting parameters $\Delta E_{\mathrm{II,I}}$ and $\Delta E_{\mathrm{III,I}}$ of the triplet term are determined. The results are given in Table 4.

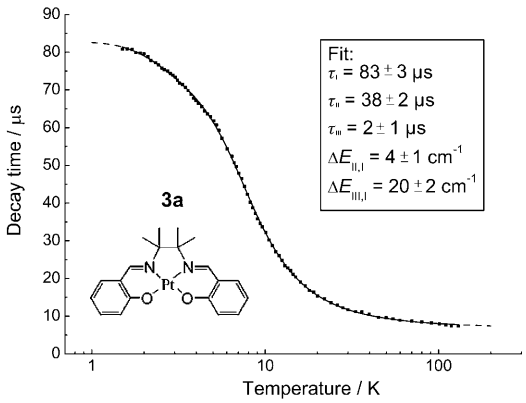

Figure 9. Plot of emission decay times of **3a** in THF ($c \approx 10^{-5}$ mol dm^{-3}) versus temperature ($\lambda_{\mathrm{ex}} = 355$ nm) and the fit of Equation (2) to the data. Inset: Energy separations and individual decay times obtained from the fit.

Table 4. Zero-field splitting (ZFS) parameters and individual decay times of the three T_1 substates I, II, and III for **3a**, **3c**, **3d**, **4b**, and **5a** measured in THF. Additional measurements for **3a** and **5a** in ethanol.

	Solvent	ZFS [cm^{-1}]		Decay time [μs]		
		$E_{\mathrm{II,I}}$[a]	$E_{\mathrm{III,I}}$[b]	t_{I}[c]	t_{II}[d]	t_{III}[e]
3a	THF	4	20	83	38	2
3c	THF	3	18	79	42	2
3d	THF	4	18	64	36	2
4b	THF	5	14	83	17	5
5a	THF	3	28	54	28	2
3a	EtOH	4	17	90	45	3
5a	EtOH	4	28	61	33	3

[a] Estimated error: ±1 cm^{-1}. [b] Estimated error: ±2 cm^{-1}. [c] Estimated error: ±3 μs. [d] Estimated error: ±2 μs. [e] Estimated error: ±1 μs.

Organic light-emitting diodes (OLEDs): The OLED structure and HOMO/LUMO level diagram of a device with **5a** as emitting material are depicted in Figure 10. The indium tin oxide (ITO) coated glass substrate with 20 Ω per square sheet resistivity was used as transparent anode. Thin layers of NPB (4,4′-*bis*[*N*-(1-naphthyl)-*N*-phenylamino]biphenyl) and Alq_3 (tris(8-quinolinato)aluminium) were used as the

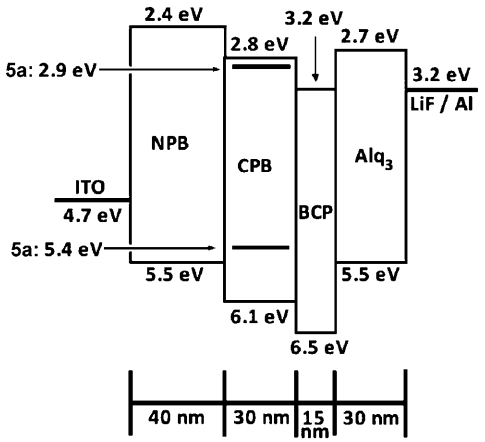

Figure 10. The device structure and energy level diagram of an OLED using **5a** as emitting material.

hole- and electron-transporting layer, respectively. CBP (4,4′-*N*,*N*′-dicarbazolebiphenyl) was chosen as the host material because its emission spectrum overlaps with the absorption spectra of the platinum(II) complexes in this work. The HOMO level of CPB is 0.6 eV lower than that of Alq_3, and the HOMO level of **5a** is similar to Alq_3, hence the excitons can easily escape from the CPB (emissive) layer to the Alq_3 layer. To enhance the device efficiency, the emission zone was confined to the CBP layer by inserting a hole blocking layer of 15 nm BCP (2,9-dimethyl-4,7-diphenyl-1,10-phenanthroline) between the CBP and Alq_3 layers. The same device structure was also used for the other OLED studies in this work.

At low platinum(II) dopant concentrations (<5.0 wt%), the device efficiency increased with dopant concentration. However, at higher platinum(II) dopant concentrations (> 5.0 wt%), aggregate/excimer formation was found to reduce the device efficiency and affect the colour purity. Figure 11

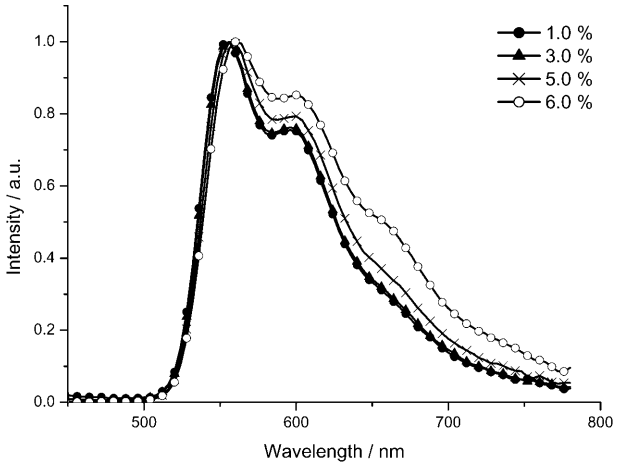

Figure 11. EL spectra of devices using **1a** with different doping concentrations.

shows the EL spectra of the devices using dopant **1a** at different concentrations. Similar studies were also performed with dopant **3a**, and the results are depicted in Figure 12. Aggregate/excimer formation was observed for a device with 5.0 wt% of **1a**, but was not evident even at 6.0 wt% of **3a**, revealing that the bulky dimethyl groups suppress the formation of excimers and/or aggregates.

The device performances using different platinum(II) Schiff base complexes as electrophosphorescent dopant materials are summarized in Table 5. Devices with the best performances were obtained at low platinum(II) dopant concentrations (1.5–4.0 wt%) for all the platinum(II) complexes.

The EL spectra of all the devices match the photoluminescence spectra of the corresponding complexes, revealing that all EL emissions come directly from the triplet excited states of the platinum(II) complexes. The devices fabricated with complexes **1a**–**4a** showed orange EL emission, which can be used to develop white OLEDs (WOLEDs). Using **1a**

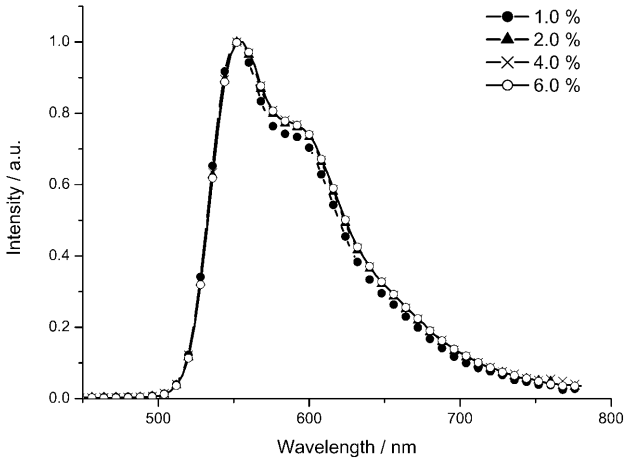

Figure 12. EL spectra of devices using **3a** with different doping concentrations.

Table 5. Device performances with best doping concentrations.

	Conc [%]	Brightness$_{max}$ [cd m^{-2}]	Efficiency$_{max}$ [cd A^{-1}]	EL λ_{max} [nm]	CIE (x,y)
1a	3	9370	6.1	554	0.49, 0.50
3a	4	23000	31	554	0.48, 0.52
4a	2	6860	3.7	552	0.48, 0.51
5a	1.5	17900	10.8	632	0.65, 0.35
5b	3	10975	1.6	628	0.65, 0.34
6	2	3060	2.2	632	0.63, 0.35
7	3	7928	1.8	628	0.65, 0.34

and $Bepp_2$ (bis[2(2′-hydroxyphenyl)pyridine]beryllium) as emitting materials, we previously reported a white OLED with CIE of (0.33, 0.35).[6] In this work, the devices fabricated with complexes **5a**–**7b** showed red emissions with CIE coordinates at around (0.65, 0.34), which are close to the red colour of the National Television Standards Committee (NTSC) (1979) standard for the cathode ray tube (CRT).

Amongst the red light-emitting materials described in this work, complex **5a** afforded the OLED with the best device performance. Figure 13 shows the EL spectra from devices using **5a** as dopant material at different applied voltages. The EL spectra showed no changes with the applied voltage, revealing excellent colour stability. Figure 14 depicts the external quantum efficiency (η_{ext}) and power efficiency (η_p) as a function of current density for the device of **5a**. Maximum η_{ext} and η_p of 9.4% and 4.9 Lm W^{-1}, respectively, have been achieved, at the current density of 8.5 mA cm^{-2} (7 V). This device showed a lifetime of more than 20000 h at 100 cd m^{-2}.

To further improve the device lifetime, the hole injection barrier was lowered by inserting a 7 nm hole injection layer of CuPc (copper phthalocyanine) between the ITO and NPB layers. CTP (9,9′-(1,1′:4′,1″-terphenyl-4,4″-diyl)dicarbazole) was chosen as the host material. The device with structure of: ITO/CuPc (7 nm)/NPB (30 nm)/CTP:**5a**/Alq_3-(30 nm)/LiF (0.3 nm)/Al (150 nm) showed a lifetime of 77000 h at 500 cd m^{-2}, which fulfilled the requirement for

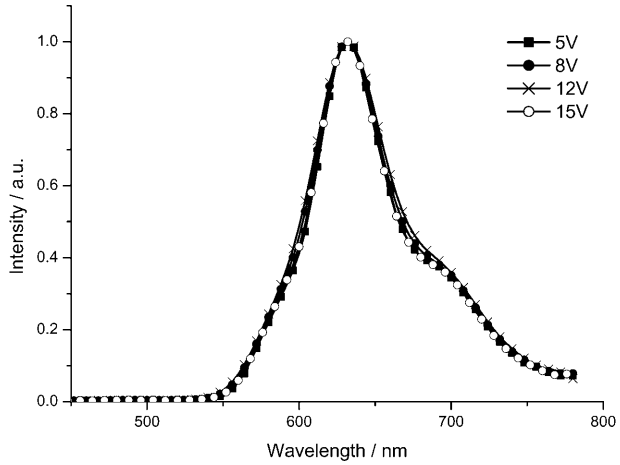

Figure 13. EL spectra of device using **5a** as emitting material at different applied voltages.

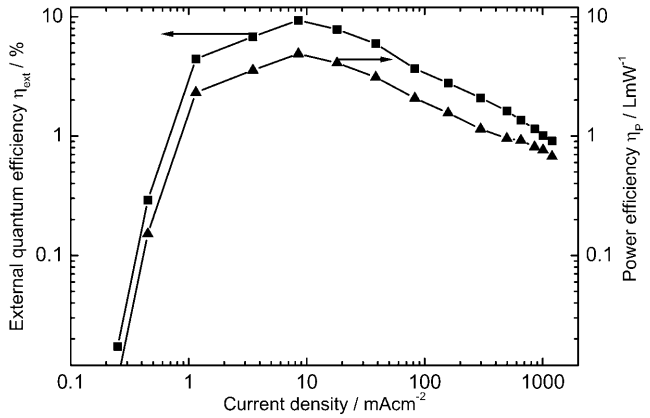

Figure 14. External quantum efficiency (■) and power efficiency (▲) as a function of current density for device using **5a** as emitting material.

use in display panels of mobile phones, MP3 players, and televisions.

Discussion

The platinum(II) Schiff base complexes are easily prepared by a one-pot reaction. They are stable towards air and moisture, are strongly photoluminescent, and have a high decomposition temperature. In general, the absorption bands of complexes **1a**–**8b** at $\lambda_{max} < 400$ nm are dominated by intraligand $\pi \rightarrow \pi^*$ transitions, and at $\lambda_{max} > 400$ nm, the absorption bands are attributed to mixed ^{1}[Pt(5d)$\rightarrow\pi^*$(Schiff base)] and intraligand ^{1}[L(phenoxide)$\rightarrow\pi^*$(imine)] charge-transfer transitions.[6] As depicted in Figures 4 and 5, the negative solvent effect on the absorption bands of **3a** and **5a** supports this assignment. This solvatochromatic effect reveals that the dipole moment of the excited state is smaller than that of the ground state, hence decreasing the solvent polarity stabilizes the excited state to a greater extent than the ground state. This finding has similarly been observed for the visible absorption bands of related N,O-ligated Pt^{II} complexes, such as [Pt(tBu$_2$N$_2$O$_2$)],[5i] [Pt(q)$_2$] (Hq = 8-hydroxyquinoline),[22] and [Pt(diimine)(dithiolate)].[23] As depicted in Table 3, the low-energy absorption band of **4a** (λ_{max} = 409 nm) blue-shifts to 394 nm (**4b**) by adding electron-withdrawing (F) substituent to phenoxide rings, but red-shifts to 439 nm (**4c**) by inserting electron-donating substituent (OMe). All these findings reveal that the HOMOs of the platinum(II) Schiff base complexes have significant parentage from the phenoxide groups.

All the platinum(II) Schiff base complexes are phosphorescent emitters. Their phosphorescence originates from mixed triplet intraligand charge transfer and metal-to-ligand charge-transfer excited states. The intraligand character in the emissive triplet excited states can be revealed by the emission spectra of the platinum(II) Schiff base complexes recorded in glassy solutions at 77 K, all of which reveal vibrational satellite structures. As an example, the 77 K MeOH/EtOH (1:4) glassy emission spectrum of **3a** at a concentration of $< 2 \times 10^{-5}$ mol dm^{-3} shows vibrational satellite bands with spacings of 1210–1440 cm^{-1}, which are characteristic of the skeletal stretching modes of Schiff base ligands. The band shapes of the emission spectra are comparable to those of related N,O-ligated platinum complexes, such as [Pt(tBu$_2$N$_2$O$_2$)][5i] (λ_{max} = 535, 575, and 620 nm; $\Delta\nu$ = 1300 and 1260 cm^{-1}) in EtOH/MeOH glassy solution at 77 K. As reported in the literature,[5i,22] the 77 K glassy emissions of these complexes are assigned to mixed ^{3}[L(phenoxide)$\rightarrow\pi^*$(imine)] and ^{3}[Pt(5d)$\rightarrow\pi^*$(L)] excited states. A mixed metal/dithiolate-to-diimine charge-transfer excited state was proposed by Eisenberg for platinum(II) diimine dithiolate complexes, which display vibronically structured emission bands in glassy *n*-butyronitrile at 77 K.[23]

As commonly observed in phosphorescent platinum(II) complexes, self-quenching of the emission and aggregate/excimer emission are encountered in the course of the spectroscopic studies of the platinum(II) Schiff base complexes. In the solid state, the emission bands of the platinum(II) Schiff base complexes are structureless, and their emission maxima λ_{max} are red-shifted from the 77 K glassy emission. The red shift in emission energy with the absence of resolved vibrational satellite structures is attributed to intermolecular interactions in the solid state.

The emissive excited triplet states: It is highly informative to ascertain the MLCT character in the emissive excited triplet states of the platinum(II) Schiff base complexes. The MLCT character in the triplet states of these platinum(II) complexes is important for OLED applications, because by this MLCT admixture spin-orbit coupling becomes effective[12,13,15,16,24] and the triplet emission lifetimes are shortened. This can lead to reductions of saturation and triplet–triplet annihilation processes. For all platinum(II) Schiff base complexes, the weak absorption shoulders near $\lambda_{max} \approx 500$ nm ($\varepsilon \approx 60$–80 mol^{-1} dm^3 cm^{-1}), and the emission bands with λ_{max} at 540–650 nm, are assigned to transitions between the lowest triplet state of mixed [L(phenoxide)$\rightarrow\pi^*$(imine)]

and [Pt(5d)→π*(L)] charge-transfer character and the singlet ground state. In frozen polycrystalline and glassy solutions, the temperature dependence of the emission lifetimes shows minute effects, consistent with the spectral assignment that the emissive excited state is not purely originated from intraligand transition.

We envisioned that detailed photophysical investigations on these platinum(II) Schiff base triplet emitters would help us understand how the structural modifications and/or electronic effects by varying R^1–R^4 substituents of Schiff base ligands affect the emission energies. The determination of ZFS values allows an estimation of the metal Pt(5d) perturbation or the metal-to-ligand charge-transfer (MLCT) character with respect to the ligand π–π* character in the triplet states. Previous reports by Yersin et al. present an ordering scheme for a correlation of ZFS values with increasing MLCT character of the emitting triplet state for libraries of luminescent compounds.[12,13,15,16] The higher the ZFS value, the more metal d-orbital involvement is present in the triplet state. This reduces the energy difference between the excited singlet and triplet states, enhances the singlet–triplet intersystem crossing rate, and lowers the emission decay time. Moreover, it leads to changes in the vibrational satellite structure, and decreases in the excited state reorganization energy, as has been shown for rigid low-temperature hosts.[12,15,16]

According to the values of the total ZFS, a classification of the degree of MLCT perturbation becomes possible. For example, $[Ir(ppy)_3]$ (ppy = 2-phenylpyridyl) exhibits a large zero-field splitting of 170 cm^{-1}.[25] Therefore, its emitting triplet state is largely of ^{3}MLCT character. A high degree of MLCT character has also been calculated for $[Ir(ppy)_3]$ in the theoretical works of Hay[26] and Nozaki.[27] Other examples of emitters with dominating MLCT character are $[Ru(bpy)_3]^{2+}$ (bpy = 2,2′-bipyridine), [Ir(4,6-dFppy)(pic)] (4,6-dFppy = 2-(4′,6′-difluorophenyl)pyridinate, pic = picolinate), and $[Os(bpy)_3]^{2+}$, with zero-field splittings of the lowest triplet state being 60,[17,18] 76,[28] and 211 cm^{-1},[17,18] respectively. In contrast, complexes such as $[Pd(thpy)_2]$ (thpy = 2-(2′-thienyl)pyridyl),[16,29] $[Pd(q)_2]$ (q = 8-quinolinato), and $[Pt(q)_2]$,[30] as well as $[Rh(bpy)_3]^{3+}$[31] and $[Pt(bpy)_2]^{2+}$[17,18], are characterized by ZFS values significantly below 1 cm^{-1}. Thus, it is concluded that these complexes emit only from perturbed ligand-centered triplet states. The heteroleptic $[Ir(ppy)_2(CO)(Cl)]$[32] and $[Re(phbt)(CO)_4]$ (phbt = 2-phenylbenzothiazole)[33] (ZFSs <1 cm^{-1}) are further representatives of this class. The intermediate range is allocated to complexes like $[Pt(thpy)_2]$,[16] [Pt(4,6-dFppy)(acac)][34] (acac = acetylacetonate), and $[Ir(btp)_2(acac)]$[35] (btp = (2-benzothienyl)pyridinate), with ZFS values of 16, 8, and 25 cm^{-1}, respectively. The emitting triplet states of these metal complexes have been assigned to ligand-centered states, which are significantly perturbed by MLCT admixtures. For $[Pt(thpy)_2]$, such an assignment was also found by ab initio calculations using the CASSCF/CASPT2 method.[36]

The complexes examined in this work show ΔE(ZFS) values between 14 and 28 cm^{-1}, and thus represent other examples of this intermediate range. The emissions of these complexes are therefore also assigned to result from ligand-centered/intra-ligand charge-transfer triplet states with significant MLCT perturbations. As depicted in Table 4, complexes **3a**, **3c**, and **3d** exhibit no considerable difference in the total zero-field splitting $\Delta E_{III,I}$ of 20, 18, and 18 cm^{-1} in THF, respectively. Comparison of **3a** with **3d** reveals that the decay time of substate I for **3d** is slightly shorter (83 μs versus 64 μs in THF). This indicates a slightly higher singlet admixture to substate I of **3d**. Considering the $\Delta E_{III,I}$ values for the other two investigated compounds, a relatively large value of 28 cm^{-1} was determined for **5a**, whereas **4b** exhibits a smaller splitting of 14 cm^{-1}. Evidently, the phenylene moiety of **5a** induces a larger MLCT perturbation to the T_1 state than the (tetramethyl)ethylene counterparts. The ZFS values obtained for **3a** and **5a** are set in relation to those of previously reported complexes in the ordering scheme depicted in Figure 15.

Complex **5a**, with the highest total ZFS value among the studied compounds, has been employed as an electrophosphorescent material for OLED fabrication. Indeed, in collaboration with Sensient Imaging Technologies GmbH, devices using **5a** as dopant material showed good device efficiency, and a device lifetime of 77,000 h at 500 cd m^{-2} has been achieved.

Conclusions

We have synthesized and studied the photophysical and electroluminescent properties of a series of platinum(II) Schiff base complexes. The low-energy absorption bands of the complexes are assigned to metal-to-ligand charge-transfer (MLCT): ^{1}[Pt(5d)→π*(L)] mixed with ^{1}[L(phenoxide)→π*(imine)] transitions. This assignment agrees with the significant MLCT perturbation in the triplet state as revealed by the total zero-field splitting (ZFS) values obtained in this work ($\Delta E_{III,I}$ = 14–28 cm^{-1}). These complexes show high emission quantum yields (0.27 for **5b**) and good thermal stability (T_d = 495 °C for **3c**).

Yellow–red organic light-emitting devices (OLEDs) were fabricated using this class of complexes as emitting materials. High-efficiency OLEDs were obtained at low doping concentration.

Experimental Section

Materials and instrumentation: All chemicals and solvents (AR grade) were used as received. Dichloromethane for photophysical studies was washed with concentrated sulfuric acid, 10% sodium hydrogen carbonate, and water, dried by calcium chloride, and distilled over calcium hydride. Acetonitrile for photophysical measurements was distilled over potassium permanganate and calcium hydride. All other solvents were of analytical grade and purified according to conventional methods.[37] Fast atom bombardment (FAB) and electron ionization (EI) mass spectra

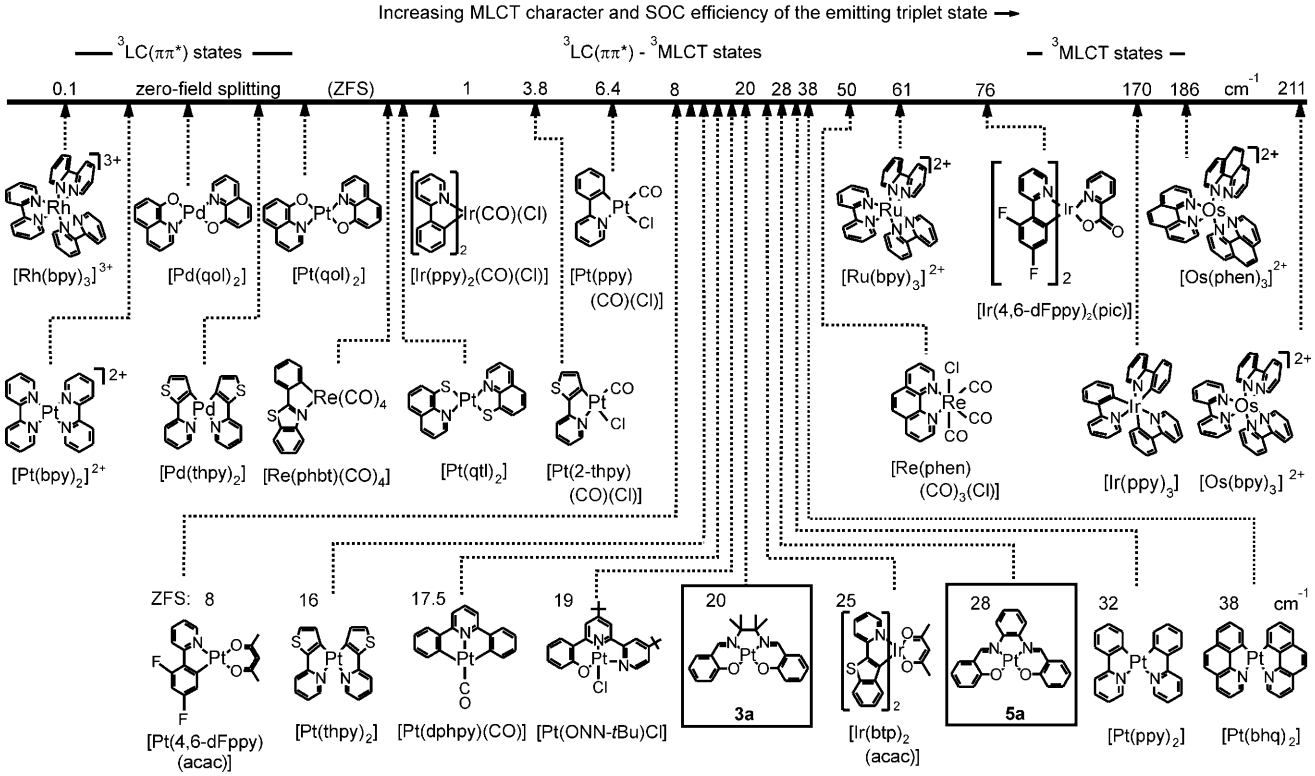

Figure 15. Ordering scheme showing metal complexes with increasing MLCT character in the emissive triplet state. Selected compounds investigated in this study (**3a** and **5a**) are marked with frames.

were obtained on a Finnigan MAT 95 mass spectrometer with a 3-nitrobenzyl alcohol matrix. ^{1}H (500 MHz) and ^{13}C (126 MHz) NMR measurements were performed on a DPX 500 Bruker FT-NMR spectrometer with chemical shifts (in ppm) relative to tetramethylsilane as reference. Elemental analyses were performed at the Institute of Chemistry of the Chinese Academy of Sciences, Beijing. UV/Vis spectra were recorded on a Hewlett Packard 8453 UV/Vis spectrophotometer.

Emission and lifetime measurements: Steady-state emission and excitation spectra were recorded on a Fluorolog-3 Model FL3–21 spectrofluorometer. Solution samples for measurements were degassed with at least four freeze-pump-thaw cycles. Low-temperature (77 K) emission spectra for glassy solutions [EtOH/MeOH (4:1 v/v)] and solid-state samples were recorded in 5 mm diameter quartz tubes, which were placed in a liquid nitrogen Dewar equipped with quartz windows. The emission spectra were corrected for monochromator and photomultiplier efficiency and for xenon lamp stability. Emission lifetime measurements were performed with a Quanta Ray DCR-3 pulsed Nd:YAG laser system (pulse output 355 nm, 8 ns). Experiments at lower temperatures were carried out in a He cryostat (Cryovac Konti Cryostat IT) in which the He gas flow, He pressure, and heating were controlled. Decay times were registered using a FAST Comtec multichannel scaler PCI card with a time resolution of 250 ps.

Luminescence quantum yields were determined by using the method of Demas and Crosby[38] with $[Ru(bpy)_3]Cl_2$ (bpy = 2,2′-bipyridine) in degassed acetonitrile as a standard reference solution ($\Phi_r = 0.062$) and calculated according to the following equation: $\Phi_s = \Phi_r(B_r/B_s)(n_s/n_r)^2(D_s/D_r)$, in which the subscripts *s* and *r* refer to sample and reference standard solution respectively, *n* is the refractive index of the solvents, *D* is the integrated intensity, and Φ is the luminescence quantum yield. The quantity *B* was calculated by $B = 1-10^{-AL}$, in which *A* is the absorbance at the excitation wavelength and *L* is the optical path length.

Time-resolved absorption difference spectroscopy was performed using the 355 nm output (third harmonic) of a Quanta-Ray Q-switched GCR-150 pulsed Nd:YAG laser as the excitation source, with the monitoring light beam generated from a 300 W Xenon lamp placed perpendicular to the excitation beam. The output of the Xenon lamp was wavelength selected by passing through a triple-grating monochromator (SpectraProR-275, 0.275 meter). The transient absorption signals were detected by a Hamamatsu R928 photomultiplier tube and amplified using a Tektronix AM502 differential amplifier, and digitised on a Tektronix model TDS 350 two-channel digital oscilloscope, interfaced to an IBM-compatible personal computer for data acquisition and analysis.

Cyclic voltammetry: Cyclic voltammetry was performed on a Princeton Applied Research Model 273 A potentiostat/galvanostat coulometer and Model 270/250 universal programmer, using a three-electrode cell system with a glassy carbon disk as the working electrode, an $Ag|AgNO_3$ (0.1 M) electrode in CH_3CN as the reference electrode, and a platinum wire as the counter electrode. Tetrabutylammonium hexafluorophosphate (0.1 M) was used as the supporting electrolyte. Ferrocenium/ferrocene was used as internal reference and all potentials were quoted with respect to $Cp_2Fe^{+/0}$.

Electroluminescence: The electroluminescent (EL) devices were prepared on patterned indium-tin-oxide (ITO) glass with a sheet resistance of 20 $\Omega\,sq^{-1}$. Thermal vacuum deposition of the materials was carried out sequentially under a vacuum of 1×10^{-6} torr in an Edwards Auto 306 system. The performance of the devices was examined using Photoresearch PR-650 in air without encapsulation. The current-voltage characteristics were studied using a Keithley 2400 sourcemeter.

Synthesis: The syntheses of [Pt(L^{1a})] (**1a**) (H_2L^{1a} = (*N,N′*-bis(salicylidene)-1,2-ethylenediamine), [Pt(L^2)] (**2**) (H_2L^2 = *N,N′*-bis(salicylidene)-1,3-propanediamine), and [Pt(L^{3a})] (**3a**) (**H_2L^{3a}** = *N,N′*-bis(salicylidene)-1,1,2,2-tetramethylethylenediamine) have been documented previously.[6,7]

[Pt(L^{1b})] (1b) (H_2L^{1b} = *N,N′*-bis(5-bromosalicylidene)-1,2-ethylenediamine)**: Complex **1b** was prepared by modification of the literature procedures.[6,7] Sodium acetate (0.082 g, 1.0 mmol) was suspended in a solution of H_2L^{1b} (0.21 g, 0.50 mmol) in DMF (15 mL). K_2PtCl_4 (0.21 g, 0.50 mmol) dissolved in DMSO (3 mL) was added dropwise to the sus-

pension at 70 °C and the resulting mixture was stirred at the same temperature for 15 h. Upon cooling, diethyl ether (50 mL) was added to the mixture to afford an orange precipitate. The solid product was filtered and washed with Et_2O (5×10 mL). Recrystallization from hot DMF afforded the product as orange crystals. Yield: 86 mg, 28%; decomposition temperature (T_d) = 315 °C; ^{1}H NMR ([D$_6$]DMSO): δ = 8.55 (s, 2H; HC=N), 7.71 (s, 2H; Ph), 7.53 (d, J = 8.9 Hz, 2H; Ph), 6.87 (d, J = 8.7 Hz, 2H; Ph), 3.83 ppm (s, 4H; CH_2); ^{13}C NMR ([D$_6$]DMSO): δ = 161.4, 155.6, 135.8, 135.0, 124.0, 123.4, 105.9, 61.2 ppm; FAB-MS: m/z: 619 [M^+]; elemental analysis calcd (%) for $C_{16}H_{12}Br_2N_2O_2Pt$: C 31.04, H 1.95, N 4.52; found: C 30.89, H 2.08, N 4.27.

[Pt(L^{3b})] (3b) (H_2L^{3b} = *N,N′*-bis(5-methylsalicylidene)-1,1,2,2-tetramethylethylenediamine): Complex **3b** was prepared by a similar procedure as that used for **3a**, but with H_2L^{3b} (0.18 g, 0.51 mmol). The crude product was purified by column chromatography using dichloromethane as eluent and evaporation of solvent from the solution gave a yellow solid. Yield: 0.14 g, 51%; T_d = 474 °C; ^{1}H NMR ($CDCl_3$): δ = 8.11 (s, 2H; HC=N), 7.30 (dd, J = 8.8, 2.2 Hz, 2H; Ph), 7.17 (d, J = 8.7 Hz, 2H; Ph), 7.13 (s, 2H; Ph), 2.28 (s, 6H), 1.51 ppm (s, 12H); ^{13}C NMR ($CDCl_3$): δ = 161.9, 151.5, 135.6, 132.5, 124.6, 122.5, 121.8, 75.8, 24.7, 19.9 ppm; FAB-MS: m/z: 545 [M^+]; elemental analysis calcd (%) for $C_{22}H_{26}N_2O_2Pt$: C 48.44, H 4.80, N 5.13; found: C 48.46, H 4.85, N 5.13.

[Pt(L^{3c})] (3c) (H_2L^{3c} = *N,N′*-bis(5-tert-butylsalicylidene)-1,1,2,2-tetramethylethylenediamine): Complex **3c** was prepared by a similar procedure as that used for **3a**, but with H_2L^{3c} (0.22 g, 0.50 mmol). Removal of solvent from the reaction mixture followed by purification through column chromatography using dichloromethane/ethyl acetate (10:1, v/v) as eluent afforded an orange-yellow solid. Yield: 0.18 g, 57%; T_d = 495 °C; ^{1}H NMR ($CDCl_3$): δ = 8.15 (s, 2H; HC=N), 7.54 (dd, J = 9.0, 2.6 Hz, 2H; Ph), 7.26 (s, 2H; Ph), 7.20 (d, J = 9.0 Hz, 2H; Ph), 1.52 (s, 12H), 1.30 ppm (s, 18H; *t*Bu); ^{13}C NMR ($CDCl_3$): δ = 161.9, 151.8, 138.1, 132.3, 128.7, 122.4, 121.2, 75.8, 33.6, 31.4, 24.7 ppm; FAB-MS: m/z: 629 [M^+]; elemental analysis calcd (%) for $C_{28}H_{38}N_2O_2Pt$: C 53.41, H 6.08, N 4.45; found: C 53.41, H 5.97, N 4.49.

[Pt(L^{3d})] (3d) (H_2L^{3d} = *N,N′*-bis(5-fluorosalicylidene)-1,1,2,2-tetramethylethylenediamine): Complex **3d** was prepared by a similar procedure as that used for **3a**, but with H_2L^{3d} (0.18 g, 0.50 mmol) to give an orange solid. Yield: 0.19 g, 69%; T_d = 484 °C; ^{1}H NMR ($CDCl_3$): δ = 8.09 (s, 2H; HC=N), 7.27–7.22 (m, 2H; Ph), 7.20–7.16 (m, 2H; Ph), 7.03 (dd, J = 9.2, 3.1 Hz, 2H; Ph), 1.53 ppm (s, 12H); ^{13}C NMR ($CDCl_3$): δ = 160.1, 154.8, 152.9, 151.1, 123.6 (d, J = 7.6 Hz), 122.5 (d, J = 23.9 Hz), 120.8 (d, J = 7.3 Hz), 116.1 (d, J = 22.3 Hz), 76.3, 24.7 ppm; FAB-MS: m/z: 554 [M^+]; elemental analysis calcd (%) for $C_{20}H_{20}F_2N_2O_2Pt$: C 43.40, H 3.64, N 5.06; found: C 43.44, H 3.68, N 4.96.

[Pt(L^{4a})] (4a) (H_2L^{4a} = *N,N′*-bis(α-methylsalicylidene)ethylenediamine): Complex **4a** was prepared by a similar procedure as that used for **3a**, but with H_2L^{4a} (0.15 g, 0.5 mmol). Recrystallization from hot DMF afforded a yellow crystalline solid. Yield: 0.11 g, 45%; T_d = 345 °C; ^{1}H NMR ([D$_6$]DMSO): δ = 7.73 (d, J = 8.3 Hz, 2H; Ph), 7.30 (t, J = 7.5 Hz, 2H; Ph), 6.89 (d, J = 8.4 Hz, 2H; Ph), 6.59 (t, J = 7.4 Hz, 2H; Ph), 3.85 (s, 4H; CH_2), 2.28 ppm (s, 6H; CH_3); ^{13}C NMR ([D$_6$]DMSO): δ = 162.9, 161.4, 131.8, 130.4, 123.4, 121.7, 115.3, 59.3, 18.6 ppm; FAB-MS: m/z: 489 [M^+]; elemental analysis calcd (%) for $C_{18}H_{18}N_2O_2Pt$: C 44.17, H 3.71, N 5.72; found: C 43.91, H 3.71, N 5.36.

[Pt(L^{4b})] (4b) (H_2L^{4b} = *N,N′*-bis(α-methyl-4-fluoro-salicylidene)ethylenediamine): Complex **4b** was prepared by a similar procedure as that used for **4a**, but with H_2L^{4b} (0.17 g, 0.50 mmol). Recrystallization from hot DMF afforded a yellow crystalline solid. Yield: 0.08 g, 29%; T_d = 379 °C; ^{1}H NMR ([D$_6$]DMSO): δ = 7.83 (t, J = 8.3 Hz, 2H; Ph), 6.63 (dd, J = 11.8, 2.8 Hz, 2H; Ph), 6.47 (td, J = 8.4, 2.8 Hz, 2H; Ph), 3.85 (s, 4H; CH_2), 2.29 ppm (s, 6H; CH_3); ^{13}C NMR ([D$_6$]DMSO): δ = 165.0, 164.6 (d, J = 13.9 Hz), 163.0, 161.1, 132.9 (d, J = 12.1 Hz), 121.0, 105.9 (d, J = 19.6 Hz), 103.7 (d, J = 22.9 Hz), 59.3, 18.3 ppm; ^{19}F NMR ([D$_6$]DMSO): δ = 109.5 ppm; FAB-MS: m/z: 525 [M^+]; elemental analysis calcd (%) for $C_{18}H_{16}F_2N_2O_2Pt \cdot H_2O$: C 39.78, H 3.34, N 5.15; found: C 40.12, H 3.23, N 5.52.

[Pt(L^{4c})] (4c) (H_2L^{4c} = *N,N′*-bis(α-methyl-5-methoxy-salicylidene)ethylenediamine): Complex **4c** was prepared by a similar procedure as that used for **3a**, but with H_2L^{4c} (0.18 g, 0.50 mmol). Removal of solvent from the reaction mixture followed by purification through column chromatography using dichloromethane/ethyl acetate (2:1, v/v) as eluent afforded an orange-yellow solid. Yield: 0.14 g, 52%; T_d = 455 °C; ^{1}H NMR ([D$_6$]DMSO): δ = 7.09 (d, J = 3.0 Hz, 2H; Ph), 7.03 (dd, J = 9.2, 3.0 Hz, 2H; Ph), 6.82 (d, J = 9.2 Hz, 2H; Ph), 3.82 (s, 4H; CH_2), 3.71 (s, 6H; OCH_3), 2.23 ppm (s, 6H; CH_3); ^{13}C NMR ([D$_6$]DMSO): δ = 160.9, 158.1, 149.1, 122.4, 122.2, 121.2, 111.9, 59.3, 55.7, 18.8 ppm; FAB-MS: m/z: 549 [M^+]; elemental analysis calcd (%) for $C_{20}H_{22}N_2O_4Pt$: C 43.72, H 4.04, N 5.10; found: C 43.32, H 4.09, N 4.98.

[Pt(L^{5a})] (5a) (H_2L^{5a} = *N,N′*-phenylenediamine): Complex **5a** was prepared by a similar procedure as that used for **3a**, but with H_2L^{5a} (0.16 g, 0.50 mmol). Removal of solvent from the reaction mixture followed by purification through column chromatography using dichloromethane/ethyl acetate (3:1, v/v) as eluent afforded a red solid. Yield: 0.21 g, 82%; T_d = 415 °C; ^{1}H NMR ([D$_6$]DMSO): δ = 9.51 (s, 2H; HC=N), 8.44 (dd, J = 4.6, 2.5 Hz, 2H; Ph), 7.86 (d, J = 5.6 Hz, 2H; Ph), 7.57 (t, J = 5.8 Hz, 2H; Ph), 7.44 (dd, J = 4.7, 2.4 Hz, 2H; Ph), 7.11 (d, J = 6.4 Hz, 2H; Ph), 6.78 ppm (t, J = 5.5 Hz, 2H; Ph); ^{13}C NMR ([D$_6$]DMSO): δ = 164.5, 151.2, 144.6, 135.6, 135.4, 127.9, 121.9, 121.2, 116.7, 116.2 ppm; FAB-MS: m/z: 510 [M^+]; elemental analysis calcd (%) for $C_{20}H_{14}N_2O_2Pt$: C 47.15, H 2.77, N 5.50; found: C 46.91, H 2.67, N 5.40.

[Pt(L^{5b})] (5b) (H_2L^{5b} = *N,N′*-bis(5-tert-butylsalicylidene)phenylenediamine): Complex **5b** was prepared by a similar procedure as that used for **3a**, but with H_2L^{5b} (0.21 g, 0.50 mmol). Removal of solvent from the reaction mixture followed by purification through column chromatography gave a deep red solid. Yield: 0.21 g, 68%; T_d = 339 °C; ^{1}H NMR ([D$_6$]DMSO): δ = 9.52 (s, 2H; HC=N), 8.45 (dd, J = 6.2, 3.4 Hz, 2H; Ph), 7.83 (d, J = 2.5 Hz, 2H; Ph), 7.68 (dd, J = 9.0, 2.5 Hz, 2H; Ph), 7.43 (dd, J = 6.3, 3.2 Hz, 2H; Ph), 7.07 (d, J = 9.0 Hz, 2H; Ph), 1.33 ppm (s, 18H; *t*Bu); ^{13}C NMR ([D$_6$]DMSO): δ = 163.0, 151.3, 144.7, 138.0, 133.9, 130.6, 127.7, 120.9, 120.8, 116.6, 33.6 (*C*Me$_3$), 31.1 ppm (C*Me$_3$*); FAB-MS: m/z: 622 [M^+]; elemental analysis calcd (%) for $C_{28}H_{30}N_2O_2Pt \cdot 0.5(CH_2Cl_2)$: C 51.54, H 4.70, N 4.22; found: C 51.55, H 4.76, N 4.58.

[Pt(L^{6})] (6) (H_2L^{6} = 1-methyl-*N,N′*-bis(salicylidene)phenylenediamine): Complex **6** was prepared by a similar procedure as that used for **3a**, but with H_2L^{6} (0.17 g, 0.51 mmol). Removal of solvent from the reaction mixture followed by purification through column chromatography using dichloromethane/ethyl acetate (3:1, v/v) as eluent afforded a red solid. Yield: 0.21 g, 81%; T_d = 411 °C; ^{1}H NMR ([D$_6$]DMSO): δ = 9.42 (s, 1H; HC=N), 9.38 (s, 1H; HC=N), 8.21–8.30 (m, 2H), 7.79–7.82 (m, 2H), 7.51–7.55 (m, 2H), 7.22 (d, J = 8.0 Hz, 1H), 7.08 (d, J = 8.7 Hz, 2H), 6.73–6.76 (m, 2H), 2.41 ppm (s, 3H; CH_3); ^{13}C NMR ([D$_6$]DMSO): δ = 164.4, 164.2, 151.0, 150.9, 150.5, 150.4, 144.5, 142.5, 138.1, 135.5, 135.4, 135.3, 135.1, 128.5, 121.9, 121.1, 121.0, 116.7, 116.2, 116.1, 20.6 ppm (CH_3); FAB-MS: m/z: 524 [M^+]; elemental analysis calcd (%) for $C_{21}H_{16}N_2O_2Pt \cdot CHCl_3$: C 41.11, H 2.67, N 4.36; found: C 41.57, H 2.86, N 4.70.

[Pt(L^{7})] (7) (H_2L^{7} = 1-*tert*-butyl-*N,N′*-bis(salicylidene)phenylenediamine): Complex **7** was prepared by a similar procedure as that used for **3a**, but with H_2L^{7} (0.19 g, 0.51 mmol). Removal of solvent from the reaction mixture followed by purification through column chromatography gave a red solid. Yield: 0.21 g, 74%; T_d = 500 °C; ^{1}H NMR ([D$_6$]DMSO): δ = 9.58 (s, 1H; HC=N), 9.46 (s, 1H; HC=N), 8.31–8.36 (m, 2H; Ph), 7.94 (dd, J = 8.1, 1.6 Hz, 1H; Ph), 7.85 (dd, J = 8.1, 1.6 Hz, 1H; Ph), 7.48–7.59 (m, 3H; Ph), 7.10 (d, J = 9.2 Hz, 2H; Ph), 6.78 (q, J = 7.1 Hz, 2H; Ph), 1.41 ppm (s, 9H; *t*Bu); ^{13}C NMR ([D$_6$]DMSO): δ = 164.4, 164.3, 151.5, 151.1, 150.7, 150.6, 144.4, 142.5, 135.7, 135.5, 135.4, 135.3, 125.1, 122.0, 121.2, 121.1, 116.2, 116.1, 116.0, 113.4, 35.0 (*C*Me$_3$), 31.1 ppm (C*Me$_3$*); FAB-MS: m/z: 567 [M^+]; elemental analysis calcd (%) for $C_{24}H_{22}N_2O_2Pt$: C 50.97, H 3.92, N 4.95; found: C 50.88, H 3.96, N 5.14.

[Pt(L^{8a})] (8a) (H_2L^{8a} = 1-fluoro-*N,N′*-bis(salicylidene)phenylenediamine): Complex **8a** was prepared by a similar procedure as that used for **3a**, but with H_2L^{8a} (0.17 g, 0.51 mmol). Removal of solvent from the reaction mixture followed by purification through column chromatography using dichloromethane/ethyl acetate (3:1, v/v) as eluent afforded a red solid. Yield: 0.16 g, 60%; T_d = 414 °C; ^{1}H NMR ([D$_6$]DMSO): δ = 9.47 (s, 1H; HC=N), 9.42 (s, 1H; HC=N), 8.34–8.48 (m, 2H; Ph), 7.82 (d, J = 8.0 Hz, 2H; Ph), 7.57 (q, J = 8.7 Hz, 2H; Ph), 7.41 (t, J = 7.8 Hz, 1H; Ph), 7.10

(dd, $J=8.6$, 2.5 Hz, 2 H; Ph), 6.78 ppm (q, $J=6.9$ Hz, 2 H; Ph); ^{13}C NMR ([D$_6$]DMSO): $\delta=165.1$, 164.4, 162.7, 160.7, 152.4, 151.6, 146.3 (d, $J=9.4$ Hz), 141.5, 136.2, 136.1, 136.0, 135.9, 122.2 (d, $J=15.6$ Hz), 121.7, 121.4, 117.7 (d, $J=9.4$ Hz), 116.9, 116.7, 114.7 (d, $J=24.3$ Hz), 104.2 ppm (d, $J=27.3$ Hz); ^{19}F NMR ([D$_6$]DMSO): $\delta=-113.6$ ppm; FAB-MS: m/z: 527 [M^+]; elemental analysis calcd (%) for $C_{20}H_{13}FN_2O_2Pt$: C 45.55, H 2.48, N 5.31; found: C 45.70, H 2.57, N 5.36.

[Pt(L^{8b})] (8b) (H$_2$L^{8b}=1-fluoro-*N*,*N*′-bis(salicylidene)phenylenediamine): Complex **8b** was prepared by a similar procedure as that used for **3a**, but with H$_2$L^{8b} (0.19 g, 0.51 mmol). Removal of solvent from the reaction mixture followed by purification through column chromatography using dichloromethane/ethyl acetate (3:1, v/v) as eluent afforded a red solid. Yield: 0.15 g, 53%; $T_d=408$ °C; ^{1}H NMR ([D$_6$]DMSO): $\delta=9.19$ (s, 1 H; HC=N), 9.14 (s, 1 H; HC=N), 8.18 (q, $J=4.8$ Hz, 1 H; Ph), 8.03 (dd, $J=10.3$, 2.5 Hz, 1 H; Ph), 7.36–7.43 (m, 4 H; Ph), 7.16 (t, $J=8.5$ Hz, 1 H; Ph), 6.95 ppm (q, $J=4.7$ Hz, 2 H; Ph); ^{13}C NMR ([D$_6$]DMSO): $\delta=162.2$, 161.5, 160.8, 160.3, 153.7 (d, $J=7.2$ Hz), 151.8 (d, $J=6.8$ Hz), 151.0, 150.3, 145.7 (d, $J=9.4$ Hz), 141.0, 124.1 (d, $J=24.9$ Hz), 123.6 (d, $J=24.7$ Hz), 122.5 (d, $J=7.8$ Hz), 122.2 (d, $J=8.0$ Hz), 120.4 (d, $J=8.5$ Hz), 120.2 (d, $J=8.4$ Hz), 117.5, 117.4 (d, $J=6.6$ Hz), 117.2, 117.1 (d, $J=10.1$ Hz),114.3 (d, $J=24.3$ Hz), 103.6 ppm (d, $J=27.5$ Hz); ^{19}F NMR ([D$_6$]DMSO): $\delta=-113.4$, -129.7, -130.0 ppm; FAB-MS: m/z: 563 [M^+]; elemental analysis calcd (%) for $C_{20}H_{11}F_3N_2O_2Pt$: C 42.64, H 1.97, N 4.97; found: C 42.70, H 2.36, N 5.16.

X-ray crystallography: Crystals of **3d**, **5a**·DMF, and **7**·CH_2Cl_2 were obtained by slow evaporation of acetonitrile of the crude samples. The crystal data and details of data collection and refinement are summarized in Table 1.

Diffraction data for **3d**, **5a**·DMF, and **7**·CH_2Cl_2 were collected on a MAR diffractometer with a 300 mm image plate detector, using graphite monochromatized $Mo_{K\alpha}$ radiation ($\lambda=0.71073$ Å). The images were interpreted and intensities integrated using the program DENZO.[39] The structures were solved by direct method employing SHELXS-97[40] on a PC. Pt and many non-H atoms were located according to the direct methods. The positions of other non-hydrogen atoms were found after successful refinement by full-matrix least-squares using program SHELXL-97[40] on a PC. For **3d**, one crystallographic asymmetric unit consists of half a formula unit, and all non-hydrogen atoms were refined anisotropically. For **5a**·DMF, one crystallographic asymmetric unit consists of one formula unit, including one DMF solvent molecule. For **7**·CH_2Cl_2, one dichloromethane solvent molecule was located and one crystallographic asymmetric unit consists of one formula unit. Non-hydrogen atoms of the solvent molecule and disordered C atoms were refined isotropically, whereas other non-hydrogen atoms were refined anisotropically.

Acknowledgements

We are grateful for the financial support from The University of Hong Kong, Nano and Advanced Materials Institute Limited (NAMI), the Innovation and Technology Commission of The Hong Kong Special Administrative Region, China (ITS/016/08NP), National Natural Science Foundation of China/Research Grants Council Joint Research Scheme (N-HKU 752/08), the Chinese Academy of Sciences-Croucher Foundation Funding Scheme For Joint Laboratories, the Research Grants Council of Hong Kong (HKU 7011/07P, HKU 7030/06P), and the German Ministry of Education and Research (BMBF). The German Academic Exchange Service (DAAD) and the German/Hong Kong Joint Research Scheme (G-HK 033/04) are acknowledged for supporting cooperation between the Hong Kong and Regensburg institutes.

[1] a) P. I. Djurovich, M. E. Thompson in *Highly Efficient OLEDs with Phosphorescent Materials* (Ed.: H. Yersin), Wiley-VCH, Weinheim, **2008**, pp. 131–161; b) H.-F. Xiang, S.-W. Lai, P. T. Lai, C.-M. Che in *Highly Efficient OLEDs with Phosphorescent Materials* (Ed.: H. Yersin), Wiley-VCH, Weinheim, **2008**, pp. 259–282; c) A. F. Rausch, M. E. Thompson, H. Yersin, *J. Phys. Chem. A* **2009**, *113*, 5927–5932.

[2] a) E. N. Jacobsen in *Catalytic Asymmetric Synthesis* (Ed.: I. Ojima), VCH, New York, **1993**, pp. 159–202; b) T. Katsuki, *Coord. Chem. Rev.* **1995**, *140*, 189–214; c) L. E. Martínez, J. L. Leighton, D. H. Carsten, E. N. Jacobsen, *J. Am. Chem. Soc.* **1995**, *117*, 5897–5898; d) M. Tokunaga, J. F. Larrow, F. Kakiuchi, E. N. Jacobsen, *Science* **1997**, *277*, 936–938; e) M. H. Wu, E. N. Jacobsen, *J. Org. Chem.* **1998**, *63*, 5252–5254; f) Z.-J. Xu, R. Fang, C. Zhao, J.-S. Huang, G.-Y. Li, N. Zhu, C.-M. Che, *J. Am. Chem. Soc.* **2009**, *131*, 4405–4417.

[3] a) Y. Hamada, T. Sano, M. Fujita, T. Fujii, Y. Nishio, K. Shibata, *Jpn. J. Appl. Phys.* **1993**, *32*, L511–L513; b) T. Sano, Y. Nishio, Y. Hamada, H. Takahashi, T. Usuki, K. Shibata, *J. Mater. Chem.* **2000**, *10*, 157–161; c) G. Yu, Y. Liu, Y. Song, X. Wu, D. Zhu, *Synth. Met.* **2001**, *117*, 211–214.

[4] a) J. L. Reddinger, J. R. Reynolds, *Macromolecules* **1997**, *30*, 673–675; b) O. Lavastre, I. Illitchev, G. Jegou, P. H. Dixneuf, *J. Am. Chem. Soc.* **2002**, *124*, 5278–5279; c) A. C. W. Leung, J. H. Chong, B. O. Patrick, M. J. MacLachlan, *Macromolecules* **2003**, *36*, 5051–5054.

[5] a) D. F. O′Brien, M. A. Baldo, M. E. Thompson, S. R. Forrest, *Appl. Phys. Lett.* **1999**, *74*, 442–444; b) V. Cleave, G. Yahioglu, P. Le Barny, R. H. Friend, N. Tessler, *Adv. Mater.* **1999**, *11*, 285–288; c) S.-C. Chan, M. C. W. Chan, Y. Wang, C.-M. Che, K.-K. Cheung, N. Zhu, *Chem. Eur. J.* **2001**, *7*, 4180–4190; d) C. Adachi, M. A. Baldo, S. R. Forrest, S. Lamansky, M. E. Thompson, R. C. Kwong, *Appl. Phys. Lett.* **2001**, *78*, 1622–1624; e) V. Adamovich, J. Brooks, A. Tamayo, A. M. Alexander, P. I. Djurovich, B. W. D′Andrade, C. Adachi, S. R. Forrest, M. E. Thompson, *New J. Chem.* **2002**, *26*, 1171–1178; f) W. Lu, B.-X. Mi, M. C. W. Chan, Z. Hui, N. Zhu, S.-T. Lee, C.-M. Che, *Chem. Commun.* **2002**, 206–207; g) B. W. D′Andrade, J. Brooks, V. Adamovich, M. E. Thompson, S. R. Forrest, *Adv. Mater.* **2002**, *14*, 1032–1036; h) C.-M. Che, Y.-J. Hou, M. C. W. Chan, J. Guo, Y. Liu, Y. Wang, *J. Mater. Chem.* **2003**, *13*, 1362–1366; i) Y.-Y. Lin, S.-C. Chan, M. C. W. Chan, Y.-J. Hou, N. Zhu, C.-M. Che, Y. Liu, Y. Wang, *Chem. Eur. J.* **2003**, *9*, 1263–1272; j) B.-P. Yan, C. C. C. Cheung, S. C. F. Kui, H.-F. Xiang, V. A. L. Roy, S.-J. Xu, C.-M. Che, *Adv. Mater.* **2007**, *19*, 3599–3603; k) M. Cocchi, J. Kalinowski, D. Virgili, J. A. G. Williams, *Appl. Phys. Lett.* **2008**, *92*, 113302; l) M. Cocchi, J. Kalinowski, V. Fattori, J. A. G. Williams, L. Murphy, *Appl. Phys. Lett.* **2009**, *94*, 073309.

[6] C.-M. Che, S.-C. Chan, H.-F. Xiang, M. C. W. Chan, Y. Liu, Y. Wang, *Chem. Commun.* **2004**, 1484–1485.

[7] a) M. E. Ivanova, G. A. Shagisultanova, *Russ. J. Phys. Chem.* **1991**, *65*, 1563–1567; b) L. P. Ardasheva, G. A. Shagisultanova, *Russ. J. Inorg. Chem.* **1998**, *43*, 85–91; c) L. P. Ardasheva, G. A. Shagisultanova, *Russ. J. Inorg. Chem.* **1999**, *44*, 711–717.

[8] E. Cesarotti, A. Pasini, R. Ugo, *J. Chem. Soc. Dalton Trans.* **1981**, 2147–2152.

[9] W. Sawodny, U. Thewalt, E. Potthoff, R. Ohl, *Acta Crystallogr. Sect. C* **1999**, *55*, 2060–2061.

[10] J. J. Novoa, G. Aullón, P. Alemany, S. Alvarez, *J. Am. Chem. Soc.* **1995**, *117*, 7169–7171.

[11] a) S.-W. Lai, M. C.-W. Chan, T.-C. Cheung, S.-M. Peng, C.-M. Che, *Inorg. Chem.* **1999**, *38*, 4046–4055; b) W. Lu, N. Zhu, C.-M. Che, *Chem. Commun.* **2002**, 900–901; c) S.-W. Lai, H.-W. Lam, W. Lu, K.-K. Cheung, C.-M. Che, *Organometallics* **2002**, *21*, 226–234.

[12] H. Yersin, W. J. Finkenzeller in *Highly Efficient OLEDs with Phosphorescent Material* (Ed.: H. Yersin), Wiley-VCH, Weinheim, **2008**, pp. 1–98.

[13] A. F. Rausch, H. H. H. Homeier, H. Yersin, *Top. Organomet. Chem.* **2010**, DOI: 10.1007/3418 2009 6.

[14] T. Azumi, H. Miki, *Top. Curr. Chem.* **1997**, *191*, 1–40.

[15] H. Yersin, *Top. Curr. Chem.* **2004**, *241*, 1–26.

[16] H. Yersin, D. Donges, *Top. Curr. Chem.* **2001**, *214*, 81–186.

[17] H. Yersin, W. Humbs, J. Strasser, *Coord. Chem. Rev.* **1997**, *159*, 325–358.

[18] H. Yersin, W. Humbs, J. Strasser, *Top. Curr. Chem.* **1997**, *191*, 153–249.

[19] R. W. Harrigan, G. A. Crosby, *J. Chem. Phys.* **1973**, *59*, 3468–3476.
[20] D. R. Striplin, G. A. Crosby, *Coord. Chem. Rev.* **2001**, *211*, 163–175.
[21] W. J. Finkenzeller, H. Yersin, *Chem. Phys. Lett.* **2003**, *377*, 299–305.
[22] R. Ballardini, G. Varani, M. T. Indelli, F. Scandola, *Inorg. Chem.* **1986**, *25*, 3858–3865.
[23] S. D. Cummings, R. Eisenberg, *J. Am. Chem. Soc.* **1996**, *118*, 1949–1960.
[24] A. F. Rausch, H. H. H. Homeier, P. I. Djurovich, M. E. Thompson, H. Yersin, *Proc. SPIE-Int. Soc. Opt. Eng.* **2007**, *6655*, 66550F.
[25] T. Hofbeck, H. Yersin, 3rd International Symposium on Molecular Materials—MOLMAT, Book of Abstracts; Toulouse, **2008**, p. 157.
[26] P. J. Hay, *J. Phys. Chem. A* **2002**, *106*, 1634–1641.
[27] K. Nozaki, *J. Chin. Chem. Soc.* **2006**, *53*, 101–112.
[28] A. F. Rausch, M. E. Thompson, H. Yersin, *Inorg. Chem.* **2009**, *48*, 1928–1937.
[29] M. Glasbeek, R. Sitters, E. van Veldhoven, A. von Zelewsky, W. Humbs, H. Yersin, *Inorg. Chem.* **1998**, *37*, 5159–5163.
[30] D. Donges, J. K. Nagle, H. Yersin, *Inorg. Chem.* **1997**, *36*, 3040–3048.
[31] M. Glasbeek, *Top. Curr. Chem.* **2001**, *213*, 95–142.
[32] W. J. Finkenzeller, P. Stößel, H. Yersin, *Chem. Phys. Lett.* **2004**, *397*, 289–295.
[33] R. Czerwieniec, W. J. Finkenzeller, T. Hofbeck, A. Starukhin, A. Wedel, H. Yersin, *Chem. Phys. Lett.* **2009**, *468*, 205–210.
[34] A. F. Rausch, M. E. Thompson, H. Yersin, *Chem. Phys. Lett.* **2009**, *468*, 46–51.
[35] W. J. Finkenzeller, T. Hofbeck, M. E. Thompson, H. Yersin, *Inorg. Chem.* **2007**, *46*, 5076–5083.
[36] K. Pierloot, A. Ceulemans, M. Merchán, L. Serrano-Andrés, *J. Phys. Chem. A* **2000**, *104*, 4374–4382.
[37] D. D. Perrin, W. L. F. Armarego, D. R. Perrin, *Purification of Laboratory Chemicals*, 2nd Ed., Pergamon, Oxford, **1980**.
[38] J. N. Demas, G. A. Crosby, *J. Phys. Chem.* **1971**, *75*, 991–1024.
[39] Z. Otwinowski, W. Minor, *Methods Enzymol.* **1997**, *276*, 307–326.
[40] G. M. Sheldrick, **1997**, SHELX97, programs for Crystal Structure Analysis, University of Göttingen, Germany.

Received: August 5, 2009
Published online: December 10, 2009

